Naval Research Laboratory
Washington, DC 20375-5320

U.S. NAVAL RESEARCH LABORATORY

NRL/7220/MR—2022/3

Demonstrate the Use of Satellite Whitecap Fraction Retrievals for Air-Sea Interaction Products in Navy Operational Models

MAGDALENA D. ANGUELOVA

Remote Sensing Physics Branch
Remote Sensing Division

MICHAEL H. BETTENHAUSEN

Remote Sensing Physics Branch
Remote Sensing Division

EDWARD J. HYER

Meteorological Applications Development Branch
Marine Meteorology Division

CHRISTOPHER P. CAMACHO

Meteorological Applications Development Branch
Marine Meteorology Division

October 24, 2022

REPORT DOCUMENTATION PAGE

Form Approved
OMB No. 0704-0188

1. REPORT DATE *(DD-MM-YYYY)*	**2. REPORT TYPE**	**3. DATES COVERED** *(From - To)*
24-10-2022	NRL Memorandum Report	4/26/2021 – 09/30/2022

4. TITLE AND SUBTITLE

Demonstrate the Use of Satellite Whitecap Fraction Retrievals for Air-Sea Interaction Products in Navy Operational Models

5a. CONTRACT NUMBER

5b. GRANT NUMBER

5c. PROGRAM ELEMENT NUMBER
NISE

6. AUTHOR(S)

Magdalena D. Anguelova, Michael H. Bettenhausen, Edward J. Hyer, and Christopher P. Camacho

5d. PROJECT NUMBER

5e. TASK NUMBER

5f. WORK UNIT NUMBER
4X29

7. PERFORMING ORGANIZATION NAME(S) AND ADDRESS(ES)

Naval Research Laboratory
4555 Overlook Avenue, SW
Washington, DC 20375-5320

Naval Research Laboratory
Marine Meteorology Division
7 Grace Hopper Ave
Monterey, CA 93943

8. PERFORMING ORGANIZATION REPORT NUMBER

NRL/7220/MR--2022/3

9. SPONSORING / MONITORING AGENCY NAME(S) AND ADDRESS(ES)

Naval Research Laboratory
4555 Overlook Avenue, SW
Washington, DC 20375-5320

10. SPONSOR / MONITOR'S ACRONYM(S)

NRL-NISE

11. SPONSOR / MONITOR'S REPORT NUMBER(S)

12. DISTRIBUTION / AVAILABILITY STATEMENT

DISTRIBUTION STATEMENT A: Approved for public release; distribution is unlimited.

13. SUPPLEMENTARY NOTES

14. ABSTRACT

This Memorandum report documents the work done for a NISE Type 2 project aiming to demonstrate that the use of satellite retrievals of whitecap fraction in the operational Navy Aerosol Analysis and Prediction System (NAAPS) can provide a new capability for air-sea products necessary for the Navy forecasts at multiple time scales. The results show that the NISE project has successfully completed the objectives and raised the Technology Readiness Level of the whitecap retrieval algorithm from level 5 to level 6, thus supporting future transition efforts.

15. SUBJECT TERMS

Numerical weather prediction, operational NAAPS, satellite data, near-real-time products, whitecap fraction, sea spray production, air-sea interaction products, WindSat, AMSR2, tropical storm intensification, coupled ocean-atmosphere models

16. SECURITY CLASSIFICATION OF:			**17. LIMITATION OF ABSTRACT**	**18. NUMBER OF PAGES**	**19a. NAME OF RESPONSIBLE PERSON**
					Magdalena Anguelova
a. REPORT	**b. ABSTRACT**	**c. THIS PAGE**	U	40	**19b. TELEPHONE NUMBER** *(include area code)*
U	U	U			(202) 404-6342

This page intentionally left blank.

CONTENTS

This page intentionally left blank.

DEMONSTRATE THE USE OF SATELLITE WHITECAP FRACTION RETRIEVALS FOR AIR-SEA INTERACTION PRODUCTS IN NAVY OPERATIONAL MODELS

1 INTRODUCTION

Air-sea fluxes quantify the transfers of momentum, heat, and mass between the ocean and atmosphere [1]. Representing the boundary conditions in coupled ocean-atmosphere models, the various air-sea fluxes and their accuracy are critical to ensure skillful forecasts on multiple time scales (days, weeks, months, years, decades) needed for Navy strategic planning [2]. The accuracy of the air-sea fluxes in current models is degraded under moderate and higher wind speeds (around and above 5-9 m s^{-1}) when the waves start to break and create whitecaps, bubble plumes, and sea spray (Fig. 1). Whitecaps, bubbles, and sea spray provide additional pathways for air-sea transfer, thereby enhancing all exchanges across the air-sea interface and the turbulent mixing in the upper ocean [3]. However, these enhancements are poorly modeled due to lack of data under high wind conditions in the open ocean [4].

Fig. 1 — Whitecaps formed by breaking waves under high wind conditions in the open ocean.

Sea spray forms in the marine environment through two mechanisms (Fig. 2). Bubble-mediated sea spray is produced indirectly when the bubbles below the breaking waves rise to the surface due to buoyancy and burst into droplets. Bubbles forming the whitecaps also burst and form a cloud of droplets above the breaking wave crests. For wind speeds above 9 m s^{-1}, this indirect mechanism is complemented with droplets directly torn off the wave crests.

The sea spray production flux must be accurately estimated to meet Navy needs for aerosol characterization, simulation, and forecasting [2]. For example, aerosol extinction is necessary to assess visibility (Fig. 3) and electro-optical propagation in the marine atmosphere. The sea spray enthalpy (the sum of the spray-mediated turbulent latent and sensible heat fluxes) is necessary for operational forecasts

Manuscript approved October 7, 2022.

of the upper ocean heat exchange, which affects predictions of tropical cyclone (TC) intensification [5, 6], a Department of Defense (DoD) Satellite-based Environmental Monitoring (SBEM) priority. Breaking waves contribute to the ambient noise in the ocean and to the turbulent heat fluxes in the sound channels. Monitoring breaking waves (in the form of whitecaps) is thus important for anti-submarine warfare (ASW). Finally, any predictive model needs a data assimilation system built on a sound, physics-based ocean surface model. Realistic ocean surface modeling accounts for the effects of the sea surface roughness and sea foam (whitecaps). However, observations to constrain these ocean surface processes in models are currently insufficient due to observation difficulties.

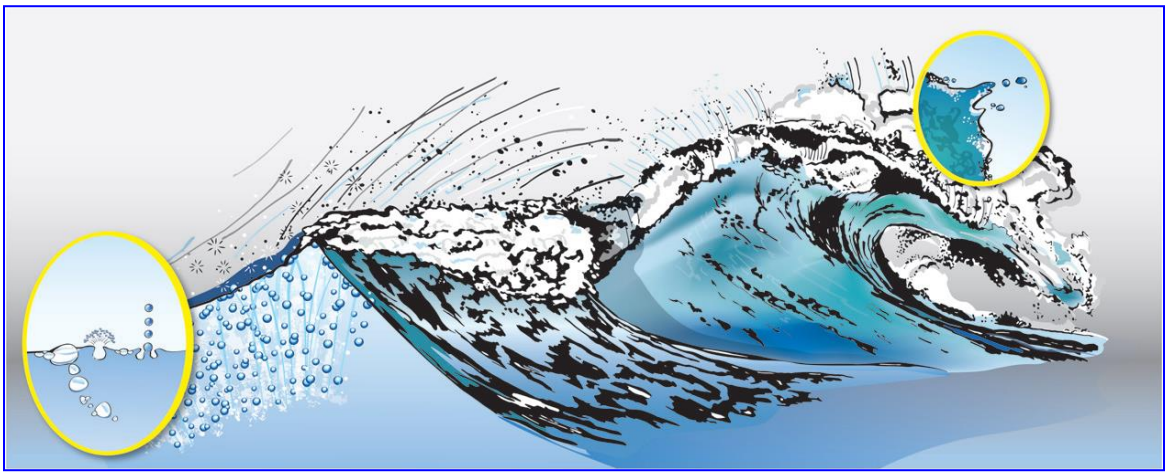

Fig. 2 — Mechanisms for sea spray formation from breaking waves (from [7]).

Fig. 3 — Sea spray is a major contributor to total AOD necessary to assess the visibility in marine atmosphere.

The Navy Aerosol Analysis and Prediction System (NAAPS) and Coupled Atmosphere/Ocean Mesoscale Prediction System (COAMPS) are two of the Navy operational numerical weather prediction (NWP) systems, both developed at the Naval Research Laboratory (NRL). NAAPS and COAMPS provide predictions of aerosols and TCs on global and regional scales. Currently, their products do not include the enhancement of the air-sea processes due to breaking waves. For example, the prediction of TC intensification uses the turbulent heat fluxes but does not account for the enthalpy due to sea spray.

Air-sea processes and fluxes associated with whitecaps, bubbles, and sea spray are usually parameterized in terms of whitecap fraction W (defined as the ocean surface covered by sea foam, Fig. 1). Typically, W is parameterized as a function of wind speed at 10 m reference height U_{10} using in situ W datasets for calibration. Figure 4 compares recent in situ measurements of W (green symbols, [8]) and one widely used $W(U_{10})$ parameterization (red symbols forming thick line) developed in 1980 using 5 in situ W data sets [9]. The in situ observations in Fig. 4 show an increase of W from 0.1% to 10% for wind speed change from 5 to 20 m s^{-1} and a spread of the same magnitude (one to two orders) at a given wind speed; e.g., W varies from ≈0.1% to ≈5% at U_{10} = 10 m s^{-1}. The $W(U_{10})$ parameterization in Fig. 4 represents the trend of W with U_{10} well; however, it is not able to predict the W variations (spread).

The spread of the in situ W data comprises both observational error and geophysical (natural) variability of the W values. Efforts are expended to minimize the former by improving the measuring procedures and assess the latter by characterizing the effects of wind speed and other oceanographic and meteorological (METOC) variables on the formation and lifetime of the whitecaps. New parameterizations of W are thus sought that account for the wind speed and additional METOC variables such as atmospheric stability, sea surface temperature (SST), sea surface salinity (SSS), currents, and surface active materials. For this reason, many oceanographic field campaigns conducted over the past decade or so have been collecting W data concurrently with additional METOC data. Still, the available in situ W and METOC data continue to be insufficient to systematically analyze and adequately quantify the additional influences on W, and thereby improve the accuracy of the sea spray production predictions.

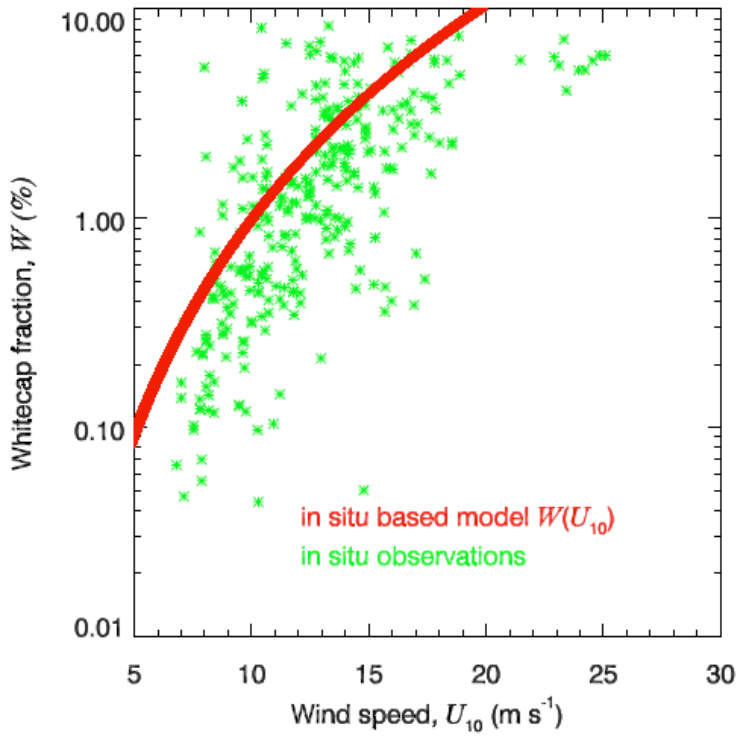

Fig. 4 — Whitecap fraction W (%) from in situ measurements (green) and from a parameterization (red) as a function of wind speed U_{10}.

As an alternative to the in situ W measurements, Remote Sensing Division (RSD, Code 7223) at NRL developed a new capability for remote sensing retrievals of W within the WindSat mission [10]. The whitecap algorithm for retrieving W from WindSat observations was implemented at RSD [11] to use with

the available WindSat data (from February 2003 to October 2020). Whether using WindSat or another satellite-borne sensor, the developed capability for remote sensing of *W* affords consistent, long-term monitoring of air-sea fluxes on a global scale [12].

Motivated by the Navy needs for improved operational models, RSD considers the transition of the whitecap algorithm to operational use pertinent. To justify such a transition, it was determined that additional work is necessary to (i) demonstrate the utility of adding this information content into modeling suites; (ii) develop analysis products suitable for near-real-time (NRT) use; and (iii) leverage data from upcoming satellite sensors.

Discussions with Naval Oceanographic Office (NAVO) clarified that the most probable framework for use of *W* and *W*-based products are the operational NAAPS and/or COAMPS run at Fleet Numerical Meteorology and Oceanography Center (FNMOC). Coordination between RSD and NRL Monterey (NRLMRY, Code 7544) on this topic led to a NISE (Naval Innovative Science and Engineering) proposal by a collaborative team from RSD and NRLMRY. The NISE project is a Type 2 Demonstration project aiming to conduct the necessary work to introduce the whitecap algorithm in the operational NAAPS in two phases, Phase 1 in fiscal year 2021 (FY21) (5 months) and Phase 2 in FY22. This memorandum report documents the results for each phase of this Demonstration NISE Type 2 project.

2 OBJECTIVE

The **overarching goal** of this effort is to adapt the WindSat algorithm for retrieving whitecap fraction to current and upcoming satellite sensors and transition it to operational use. Operational *W* retrievals can then serve as a basis for improving existing and adding new sea spray related products from Navy operational systems.

The **objective specific** to this NISE project is to demonstrate new capability in the operational NAAPS for air-sea products by incorporating an algorithm for NRT satellite whitecap fraction retrievals from AMSR2 and using these whitecap retrievals to calculate sea spray production.

The chart in Fig. 5 visualizes the flow of planned activities necessary to achieve these objectives.

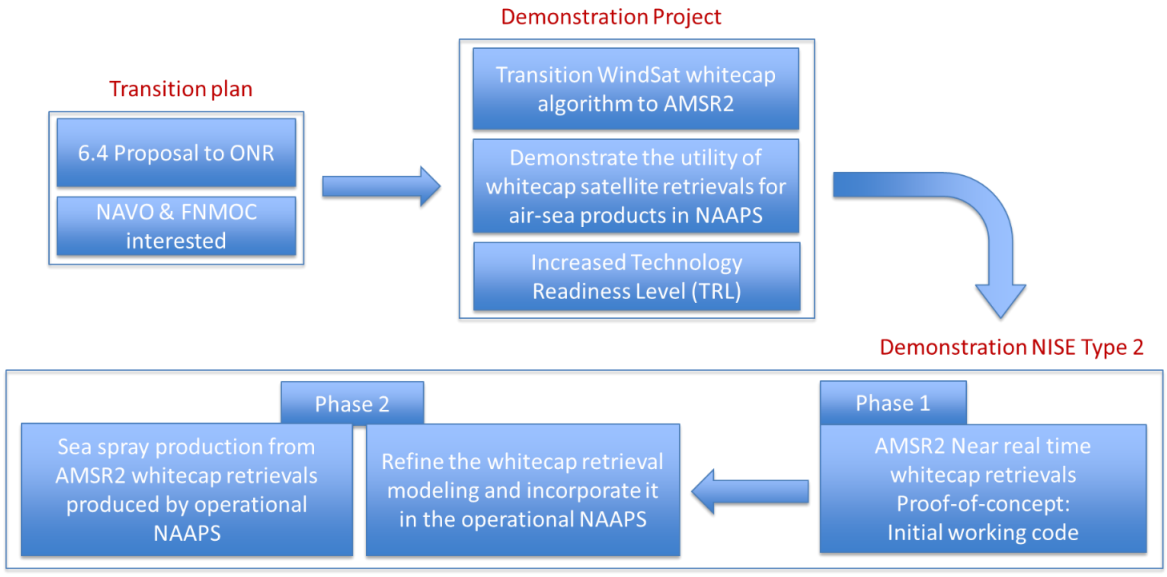

Fig. 5 — Planned activities necessary to achieve the goals of this NISE project as a part of overall transition effort.

FNMOC is responsible for the operational runs of NAAPS, COAMPS, and other Navy NWP models. NRLMRY supports development of these models (including development, implementation, and testing) and upgraded model capabilities, and preparation of updated models for transition to Navy operations. In this report we use "operational NAAPS" for the research NAAPS at NRLMRY because it is the testbed for transitions to the operational NAAPS at FNMOC.

2.1 Demonstration using NAAPS

As stated in the transition objectives (Section 2), we aim to demonstrate that the addition of a new capability to NAAPS that accounts for the variability of the air-sea fluxes has the potential to improve the existing Navy's operational forecasts and provide additional stand-alone products.

NAAPS is used to operationally predict vertically resolved aerosol extinction from scattering and absorption, which includes contributions from sea spray aerosols and other aerosol species. NAAPS obtains the sea spray production using the $W(U_{10})$ parameterization shown in Fig. 4 (red symbols). Figure 6 shows an example of aerosol optical depth (AOD, the vertical integral of aerosol extinction) due specifically to sea salt aerosols obtained with the same $W(U_{10})$ parameterization. As discussed for Fig. 4, this $W(U_{10})$ yields

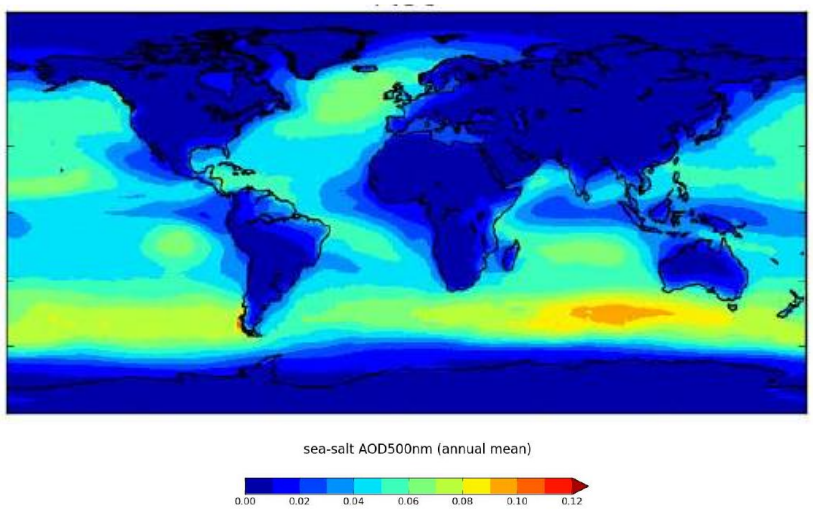

Fig. 6 — Annual mean values (over a 5 yr period 2002–2006) of sea spray AOD at 500 nm obtained with the $W(U_{10})$ parameterization shown in Fig. 4. (From [13]).

sea spray AOD which does not include the influence of other factors, besides the wind speed, on W and thus the sea spray production. Using satellite retrievals of W (or multi-variable W parametrizations based on such retrievals) will afford accounting for the factors affecting whitecaps and sea spray in different regions on the globe. We aim to assess how much the satellite W retrievals will affect the sea spray contribution to the NAAPS total AOD and whether the changes improve (or not) the AOD predictions.

Figure 7 shows a daily map of whitecap fraction retrieved from WindSat observations. Adapting the whitecap algorithm to the AMSR2 sensor will provide daily global maps of W like the one in Fig. 7. This daily whitecap fraction imagery is a stand-alone new product that can be generated both in NRT and from archival data and can therefore be used to show real world influence of wind speed **and** METOC factors on retrieved W. Besides daily imagery of sea spray production, such whitecap fraction maps can be used to provide other new products, including daily maps (imagery) of surface albedo due to whitecaps, sea spray-mediated heat fluxes, gas exchange enhancement due to bubbles and sea spray.

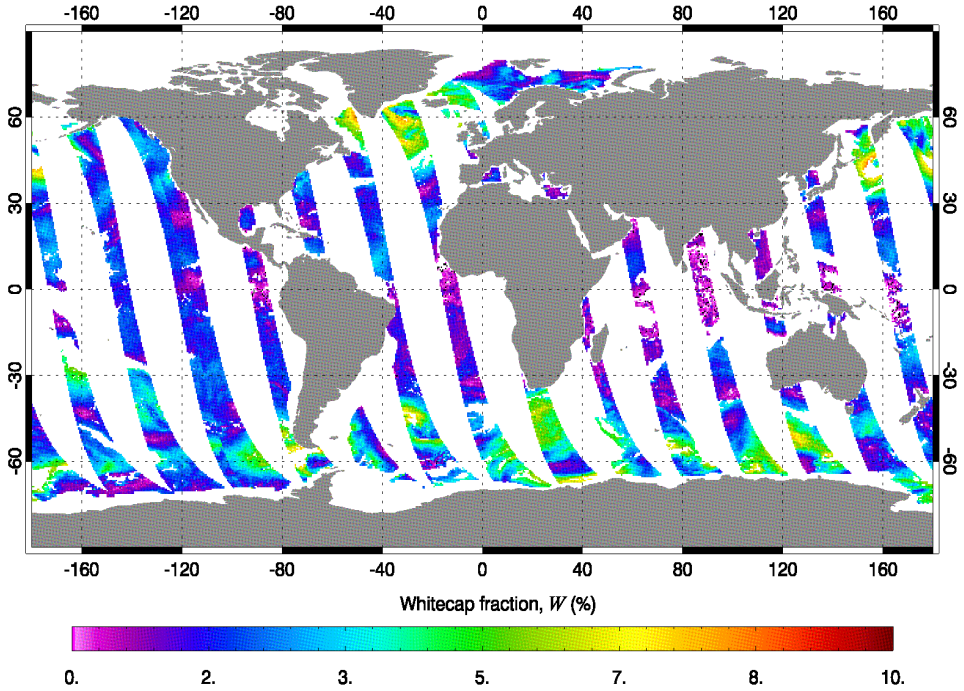

Fig. 7 — Daily map of whitecap fraction retrieved from WindSat observations at 37 GHz, H pol.

2.2 Focus on AMSR2 observations

As stated in the transition objectives (Section 2), in this project we focus on adapting the WindSat whitecap algorithm to AMSR2 sensor. This is well justified decision for several reasons.

First, AMSR2 is presently operational. Its frequency channels track well with those of WindSat—now a non-operational, heritage sensor, and WSF–M—an upcoming sensor, which represents the next generation of DoD microwave sensors. Table 1 shows the frequency bands, the polarizations, and the earth incidence angles (EIAs) for WindSat, AMSR2, and WSF–M. The cartoon in Fig. 8 visualizes the definition of EIA.

Table 1 — Frequency bands, polarizations, and EIAs for three satellite-borne microwave sensors. Polarization notations: V and H for linear vertical and horizontal polarizations; ±45° for linear polarizations at +45° and –45°; LCP/RCP for left- and right-handed circular polarizations.

Sensor specifications	**WindSat**	**AMSR2**	**WSF–M**
Status	Heritage	Operational	Upcoming
Frequency bands (GHz)	6.8, 10.7, 18.7, 23.8, 37	6.925, 7.3, 10.65, 18.7, 23.8, 36.5, 89	10.85, 18.85, 23.8, 36.75, 37.3, 89
Polarization	V, H, +45°, –45°, LCP, RCP	V, H	V, H, +45°, –45°, LCP, RCP
EIA range	49°–54°	54°–56°	Not available

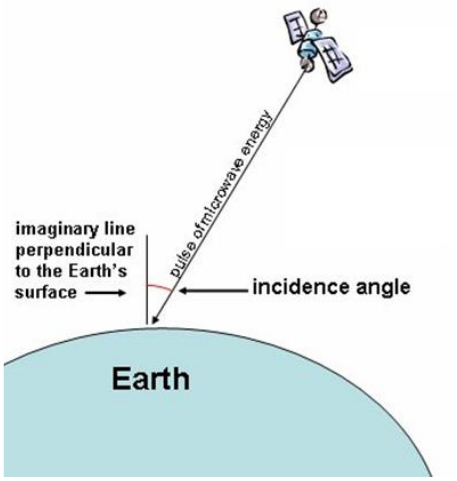

Fig. 8 — Definition of earth incidence angle for observing ocean surface phenomena from a satellite.

Second, AMSR2 data are presently ingested by NAVO and FNMOC. This will support near term transition to operations.

However, AMSR2 differs from WindSat in the EIA range (Table 1) and in sensor calibration specifics. These differences require a plan to adjust the physical modeling and implement the code/software for the whitecap algorithm to the AMSR2 sensor parameters.

3 BACKGROUND

The work necessary to deliver on the project objectives (Section 2) was formulated on the basis of the existing status of the WindSat whitecap retrieval algorithm, the NAAPS modeling of the sea spray flux, and the specifics of the AMSR2 data. Background on these topics is given here to justify and support the approach formulated for each phase of the NISE project.

3.1 Remote sensing of whitecaps

The sea foam comprising the whitecaps has distinct remote sensing signatures in different portions of the electromagnetic (EM) spectrum [3]. The sea foam is highly reflective at visible wavelengths due to radiation scattering among the bubbles forming the foam. The scattering renders the whitecaps highly visible as bright white patches (Fig. 1). The sea foam is highly emissive at microwave frequencies due to extensive absorption in the lossy seawater content of the sea foam. The absorption and subsequent emission render the whitecaps "hot" blackbody-like spots on the ocean surface. At infrared (IR) wavelengths, the sea foam is both reflective and emissive with both signals being relatively weak. The dichotomy of the sea foam in the IR region is useful [14], but this is not a subject of this project.

The remote sensing signature underlying the in situ observations of whitecaps with video cameras from ships and towers is their high reflectance in the visible. For satellite observations of whitecaps, the choice of sea foam remote sensing signature depends on the efforts needed to overcome the atmospheric effects on the sea foam signal. Via scattering and absorption, the atmosphere strongly attenuates the EM radiation at visible and IR wavelengths. For this reason, satellite retrievals of geophysical variables in the visible and IR portions of the EM spectrum are limited to clear sky cases. The atmosphere attenuates the microwave radiation too [15], but the problem of accounting for this attenuation is more tractable [16]. For this reason, we have developed a remote sensing technique for whitecap detection at microwave

frequencies. The fact that by its nature the sea foam is an effective emitter [17] permits retrieval of whitecaps by passive remote sensing.

3.1.1 Whitecaps observation with microwave radiometry

Passive remote sensing uses radiometers to measure the EM radiation naturally emitted by the ocean-atmosphere system in terms of brightness temperature T_B. The schematic in Fig. 9 shows the formation of the T_B signal at the at the top of the atmosphere (TOA) that a satellite-borne microwave radiometer detects. A radiative transfer model (RTM) describes the contributions to T_B from the ocean surface and the atmosphere and their interaction via transmission, quantified with t, emission e, and reflection $r = 1 - e$.

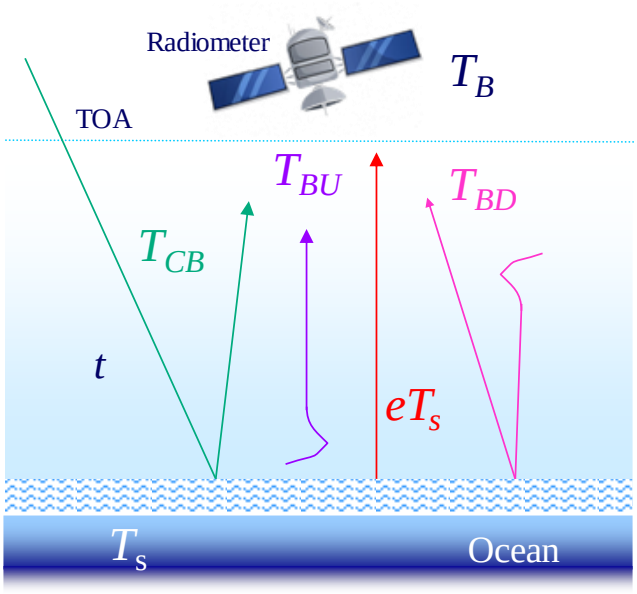

Fig. 9 — Schematic showing the atmosphere and surface contributions to T_B at the TOA measured by a satellite-borne microwave radiometer. The equation at the bottom is the RTM for T_B.

Specifically, the RTM (shown at the bottom of Fig. 9) includes the thermal emission of the ocean surface at a given SST T_s, attenuated by the atmosphere while propagating upward toward the satellite; the atmospheric upwelling radiation T_{BU}; atmospheric downwelling radiation T_{BD}, reflected (via r) from the surface toward the satellite; and cosmic background T_{CB}, transmitted (via t) through the atmosphere and reflected (r) upward toward the satellite.

The whitecap fraction is introduced in the RTM via the surface emissivity e. We represent e as a sum of two terms, which account for the effects of the foam-free rough surface e_r and foam-covered surface e_f:

$$e = e_r + e_f = (1 - W)E_r + WE_f \tag{1}$$

As (1) shows, the whitecap fraction W is a weighing factor in terms e_r and e_f for the contributions from, respectively, the roughness-only emissivity E_r and foam emissivity E_f. From (1), we obtain the geophysical model function (GMF) for whitecap fraction at the sea surface:

$$W = e_f/E_f = (e - e_r)/E_f \tag{2}$$

We use the RTM (Fig. 9) to cast (2) in terms of T_B at the TOA:

$$W = \left(T_B^{\mathrm{TOA}} - T_{Br}^{\mathrm{TOA}}\right)/\left(A\,T_{Bf}\right) \tag{3}$$

where $T_{Bf} = E_f T_s$ is the T_B of 100% foam-covered surface, while term $T_B^{\mathrm{TOA}} - T_{Br}^{\mathrm{TOA}}$ is the observed T_B due to foam at the TOA. Factor A—an expression involving the atmospheric variables t, T_{BU}, T_{BD}, and T_{CB} (Fig. 9)—is the atmospheric correction that gives term $T_B^{\mathrm{TOA}} - T_{Br}^{\mathrm{TOA}}$ at the surface.

3.1.2 WindSat whitecap algorithm

Figure 10 shows a flow chart of components comprising a whitecap retrieval algorithm based on the W GMF (3). Whitecap retrievals (purple boxes in Fig. 10) require three major elements. The first is having satellite observations for T_B^{TOA} (blue boxes in Fig. 10). Next, a suite of modeling modules is necessary for A, T_{Br}^{TOA}, and T_{Bf} (green boxes) to simulate the T_B signals from the atmosphere, sea surface roughness, and 100% foam-covered surface. A model for seawater permittivity is needed for the roughness and foam modules, and a wave spectrum model is necessary for the roughness. Finally, input data are necessary to force (drive) the modelling modules (brown boxes in Fig. 10). The model input data are a set of geophysical variables—wind vector with speed U_{10} and direction ϕ, water vapor V, cloud liquid water L, SST T_s, and SSS S—provided either by a global model (e.g., from the Navy Global Environmental Model, NAVGEM) or by satellite retrievals (also called Environmental Data Record, EDR); these two options are shown in Fig. 10 with brown arrows. This section briefly describes the modeling modules used in the whitecap algorithm. The input data are described in Section 3.1.3.

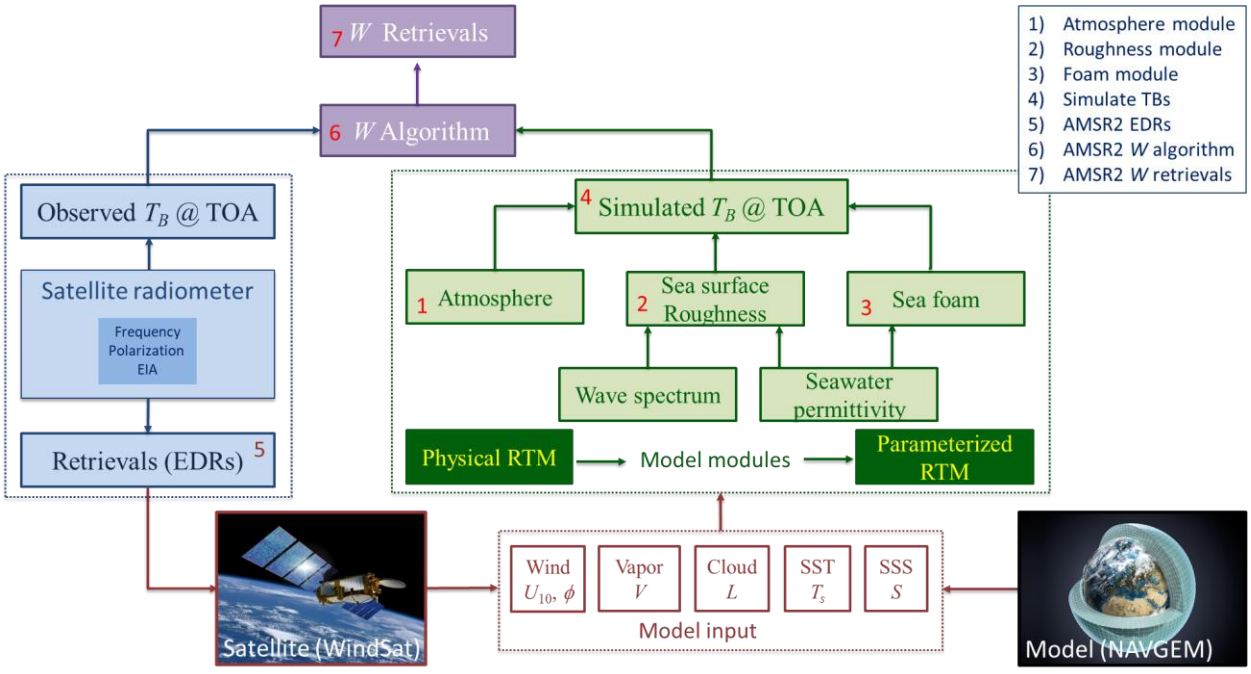

Fig. 10 — Flow chart of the elements comprising the whitecap retrieval algorithm. The 7 tasks listed (top right) and associated with the respective element in the chart (red numbers) were implemented during Phase 1 (Section 5.1).

Each modelling module in Fig. 10 comprises a physical RTM and a parameterized RTM (dark green boxes in Fig. 10). The physical RTM provides a database of physical values computed for a wide range of model parameters. Then, a parameterized RTM is developed from the physical values to ensure fast, NRT retrievals. Some of the physical RTMs are readily available, e.g., the atmospheric model. The innovative parts that were developed specifically for the WindSat whitecap algorithm are the roughness-only and sea foam models (Fig. 10).

The roughness-only term e_r in (1) can be simulated with the so-called 2-scale model [18], which was adjusted for WindSat data [19]. The 2-scale model computes the combined emissivity of short-scale waves (ripples) riding on long-scale waves (swell), a sea state exemplified in Fig. 11a. The mathematical expression for the 2-scale model is shown in Fig. 11c. The roughness-only emissivity is calculated using the scattering coefficients γ_{ab} (where subscripts *a* and *b* stand for all combinations of H and V polarizations). The expression in Fig. 11c shows that we obtain γ_{ab} by first calculating the small-scale scattering coefficients (see text for each term in Fig. 11c) in a local coordinate system, as they are modified by the probability distribution (PD) of the large-scale slopes, and subsequent transformation of the local coordinates to the mean sea surface. The expression also includes hydrodynamic modulation *m*, which accounts for the enhanced roughness on the wave face (shown with an arrow in Fig. 11b) as compared to the back of the wave. All this is averaged (integrated) over the range of large-scale slopes.

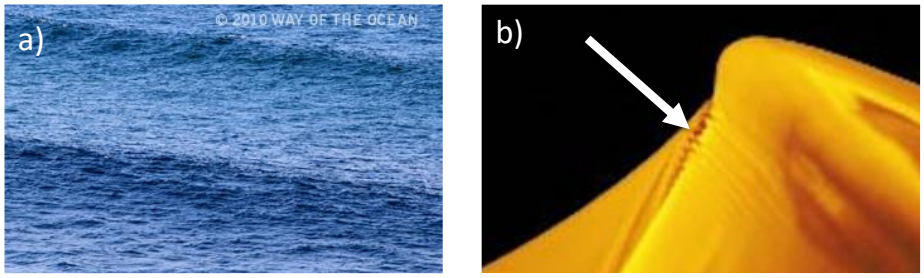

Fig. 11 — Elements of a 2-scale model: a) Short-scale waves (ripples) riding on long-scale waves (swell); b) Enhanced roughness at the wave face (shown with arrow, from [20]); c) Mathematical expressions for the 2-scale model (from [18]).

We developed a foam emissivity RTM for the WindSat mission to simulate E_f [21]. The main feature of the foam emissivity RTM is the profile of the foam void fraction f_a (the air content in the air-seawater mixture) in the foam layer depth (Fig. 12). The change of the void fraction in foam is due to the stratification of the bubbles forming the foam by size. Close to the surface, large bubbles with thin walls make foam with high air content (high f_a). Smaller bubbles close to the seawater contain less air (low f_a). The f_a profile provides a smooth transition between the vastly different permittivity properties of air and seawater. This is the physical basis for the high, blackbody-like emissivity of the foam-covered sea surface. Using the foam properties—foam layer thickness *d* and foam void fraction f_a—we build the foam emissivity RTM on a robust physical basis. This contrasts with empirical foam models, which use only sensor parameters such as frequency and EIA [21].

The WindSat foam emissivity model uses fixed values for the foam properties, namely d and the f_a limits at the upper (air-foam) and lower (foam-seawater) boundaries of the foam layer [21]. Our previous 6.1 basic research (WU 8967) showed that the f_a upper limit (v_{af}) is sensitive to variations of d and the sensor frequency. The upper void fraction limit can thus be used as a tuning parameter.

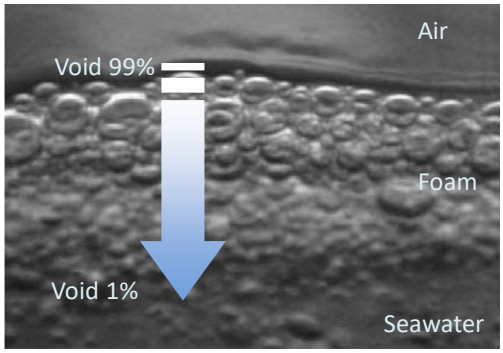

Fig. 12 — Foam layer formed by a breaking wave. Stratification of bubbles within the foam by size leads to a vertical profile of the foam void fraction with upper (air-foam) limit of 99% and lower (foam-seawater) limit of 1%.

With 6.1 (WUs 8967 and 4500) and 6.2 (WU 6A08) projects, we have implemented several versions of the whitecap algorithm using WindSat data. The versions differed in the implementation of the modelling modules and the sources for the input variables [11]. The latest version provides the best retrievals of W using both WindSat observations for term T_B^{TOA} and WindSat EDRs (U_{10}, ϕ, V, L, and T_s) as input to the models [11].

The whitecap algorithm produces W retrievals at different frequencies and polarizations. The W values at different frequencies are useful approximations for the thickness of the whitecaps. For example, W at 10 GHz represent predominantly thick foam layers formed during the active wave breaking, while W at 37 GHz includes both thick active whitecaps and thin layers of decaying foam behind the breaking waves. The polarization differences can be used as a measure for the whitecap sensitivity to wind speed forcing—stronger at H polarization and much weaker for V polarization, especially at the WindSat EIAs (Table 1)

3.1.3 Input data for the whitecap algorithm

WindSat was designed and built by NRL RSD and Space Systems Development Division (SSDD). Gaiser et al. [10] give a complete description of the WindSat sensor and data processing. Operating at 22 frequency-polarization channels (Table 1), WindSat data includes observations from forward and aft swaths with widths of about 950 and 350 km, respectively. With its polarimetric capability, WindSat is the first space-based microwave radiometer to retrieve wind vector from T_B observations. Before the WindSat launch, space-based retrieval of ocean surface vector winds was provided by scatterometers (such as the QuikScat).

The WindSat ground data processing of the raw WindSat measurements produces T_B values (in K). Specifically, the T_B values include corrections for Faraday rotation due to propagation through the ionosphere, polarization rotation, antenna cross-polarization, and spillover and along-scan biases. The measurements are collocated and averaged to provide T_B values at three different elliptical earth-based footprints resolutions: high resolution of approximately 25 km × 35 km; medium (≈ 35 km × 53 km); and low (≈ 50 km × 71 km). Finally, the WindSat data in the 22 channels are combined to provide T_B values in 16 channels for the full modified Stokes parameters [10]. The WindSat capability to form the full modified

Stokes supports the retrieval of the wind speed and direction ϕ [16]. The whitecap algorithm uses for term T_B^{TOA} in (3) the high resolution WindSat T_B values from the forward swath at dual (H and V) polarization, i.e., 10 of the 16 T_B channels.

The WindSat geophysical retrievals (EDRs) are obtained from the 16-channel T_B full Stokes observations (called a measurement vector) combined with a forward model and a nonlinear optimal estimator [16]. The retrieved quantities are given with the state vector (U_{10}, ϕ, V, L, T_s). The forward model relates the state and measurement spaces. The optimal estimator is akin to minimizing a cost function for the state vector. It iteratively estimates χ^2 as a measure for the goodness of fit of the forward model, evaluated using the retrieved state vector, to the measurement vector.

The WindSat forward model simulates the 16 T_B observations using the state vector (U_{10}, ϕ, V, L, T_s) and models for the atmosphere and the ocean surface emissivity, similar to the modeling modules shown in Fig. 10. The major difference between the models in the WindSat geophysical and whitecap retrieval algorithms is that the former represents *e* in (1) without trying to separate it into roughness-only and foam-covered terms as does the latter. Instead, the WindSat forward model represents *e* using the 2-scale model calculations with an empirical correction developed from a training WindSat dataset. The quality of the retrieved EDRs depends strongly on the quality control (QC) of both the T_B observations and the geophysical retrievals. Thus, both WindSat geophysical and whitecap retrieval algorithms implement a suite of QC flags.

The SSS input for the WindSat whitecap algorithm uses monthly salinity climatology for *S* from the World Ocean Atlas provided by the NOAA National Centers for Environmental Information.

3.2 Sea spray flux from operational NAAPS

3.2.1 Sea spray source function

The operational NAAPS calculates the total (i.e., size-integrated) sea spray mass flux *F* (in kg m^{-2} s^{-1}) of dry particles with a power law parameterization in terms of wind speed [22]:

$$F = 1.37 \times 10^{-13} U_{10}^{3.41} \tag{4}$$

Equation (4) is based on the concept of sea spray source function (SSSF) [23] for sea spray droplets with radii r_{80} at a relative humidity (RH) of 80%:

$$\frac{dF}{dr_{80}} = \frac{W}{\tau}\frac{dE}{dr_{80}} \tag{5}$$

where W is the whitecap fraction, τ is whitecap decay timescale, and dE/dr_{80} is the aerosol productivity per unit whitecap area.

The value of whitecap fraction W in (5) can be either measured or estimated. Measured W values can be obtained in situ from photographs or remotely from satellite-borne radiometers. Estimated W values are typically obtained with a power-law parameterization $W(U_{10})$ (Section 1). The operational NAAPS uses the most widely known and used parameterization [9]:

$$W(U_{10}) = aU_{10}^{b} = 3.84 \times 10^{-6} U_{10}^{3.41} \tag{6}$$

which gives *W* as a fraction (not %). Appendix A.1 gives the derivation of (4) from (5) and (6).

The derivation of (4) (Appendix A.1), shows that constant a in (6), though associated with W, is incorporated in the size distribution term (the brackets in A.1). Because of this mix-up of quantities related to the whitecap fraction parameterization and the sea spray size distribution, we cannot use (4) with different $W(U_{10})$ expressions.

Our work on a 6.2 project (WU #6A08) resolved this by clearly separating $W(U_{10})$ and the sea spray size distribution in (4). Recognizing the same wind speed term U_{10}^{b} in (4) and in (6), we re-arrange (4) as follows:

$$F = 1.37 \times 10^{-13} U_{10}^{3.41} \frac{3.84\times10^{-6}}{3.84\times10^{-6}} = [3.84 \times 10^{-6} U_{10}^{3.41}] \frac{1.37\times10^{-13}}{3.84\times10^{-6}} \quad (7)$$

Then the modified (4) (in kg m^{-2} s^{-1}) is:

$$F = W(U_{10})\ 3.56771 \times 10^{-8} \quad (8)$$

where W is a fraction (not %). Constant 3.56771×10^{-5} (in g m^{-2} s^{-1}) represents solely the integrated size distribution for dry particles from 0.2 to 4 μm. Appendix A.2 shows the explicit functional form of this sea spray size distribution.

3.2.2 Whitecap fraction parameterizations

Using (8) instead of (4) to obtain the total sea spray flux F with the operational NAAPS allows the use of different $W(U_{10})$ parametrizations besides (6). A $W(U_{10})$ parameterization based on in situ W data that has gained recognition recently is that of Brumer et al. [8]:

$$W(U_{10}) = 7.38 \times 10^{-2}(U_{10} - 4.24)^{1.42} \quad (9)$$

which gives W in %.

Two parameterizations based on satellite W retrievals have been used in models so far. The parameterization proposed by [25] is based on satellite W retrievals at 10 GHz:

$$W(U_{10}) = 4.6 \times 10^{-3} U_{10}^{2.26} \quad (10)$$

which gives W in %. Equation (10) has been adjusted and tested in an ensemble version of NAAPS (ENAAPS [26, 27]) as follows:

$$W(U_{10}) = 4.6 \times 10^{-3} U_{10}^{2.26} - 0.1 \quad (11)$$

with W in % again. The modified form (11) has been transitioned for use in the operational NAAPS run at FNMOC.

A parametrization based on WindSat W retrievals that includes SST T_s in addition to U_{10} has been proposed by [28]:

$$W(U_{10}, T_s) = a(T_s)[U_{10} - b(T_s)]^2 \quad (12)$$

$$a(T_s) = a_0 + a_1 T_s + a_2 T_s^2 \quad (12a)$$

$$b(T_s) = b_0 + b_1 T_s \quad (12b)$$

which gives *W* as a fraction (not in %). Parameterization (12) is currently in operational use in the aerosol module of the European Centre for Medium-Range Weather Forecasts (ECMWF) that provides daily global analysis and forecast of aerosols for the Copernicus Atmosphere Monitoring Service [29].

Parameterizations (9)-(12) have been derived from early versions of the whitecap algorithm, different from that currently implemented for AMSR2 observations.

3.3 Data and data processing

The AMSR2 instrument is a conical scanning radiometer operating at 14 frequency-polarization channels (Table 1). AMSR2 was launched aboard the Japan Aerospace Exploration Agency (JAXA) Global Change Observation Mission 1st-Water (GCOM-W1 or "SHIZUKU") satellite in May 2012. AMSR2 obtains data over a 1450 km swath, much wider than the WindSat forward swath (Section 3.1.3). Figure 13 shows a daily map of AMSR2 T_B data; comparison to Fig. 7 clearly shows that the AMSR2 swath is wider than that of WindSat. With ascending and descending passes, AMSR2 acquires daytime and nighttime T_B data with more than 99% coverage of the Earth every 2 days. The AMSR2 T_B data come in three levels depending on the averaging over, and gridding of, the swath raw data (Appendix B).

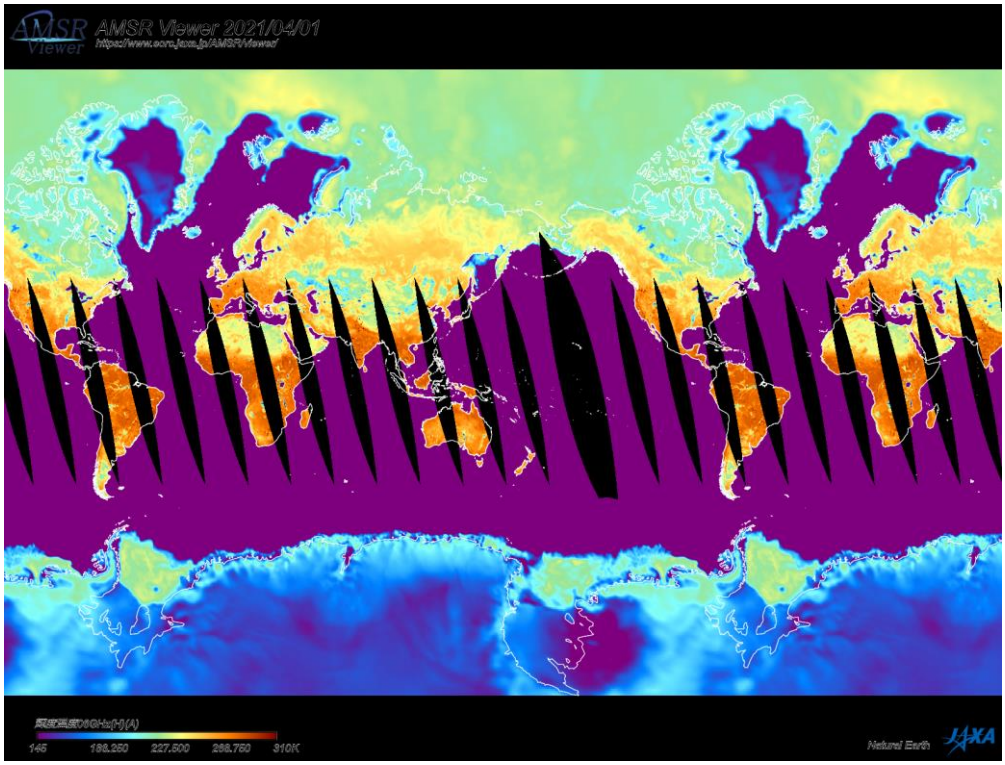

Fig. 13 — Daily map of T_B measured by AMSR2 radiometer at 6 GHz, H pol., ascending pass

In contrast to WindSat, wind speed direction ϕ cannot be retrieved from the AMSR2 T_B measurements because AMSR2 data cannot provide the full modified Stokes vector (Section 3.1.3). As Fig. 10 shows, we use global model data for input variables when satellites do not provide them. Thus, in addition to AMSR2

T_B data, we also use data from NAVGEM and the Navy Global Hybrid Coordinate Ocean Model (HYCOM).

NAVGEM is a global NWP model run by FNMOC since February 2013 [30]. Its current version 2.0 has ~17 km horizontal resolution and 60 vertical levels. NAVGEM runs four times a day with 3-hourly outputs (color-coded in Fig. 14a).

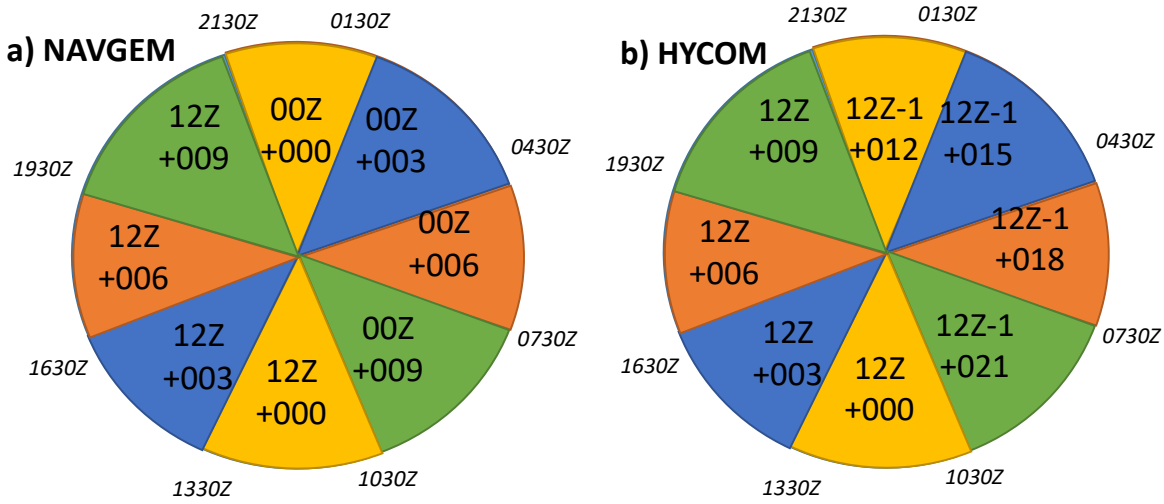

Fig. 14 — Timing of model run and output: a) NAVGEM; b) HYCOM. Meteorological fields are spatially interpolated to the satellite observation locations to produce a combined input for the *W* retrieval. For a satellite observation at a given time (indicated by its radial position from 00Z at the time to 12Z at the bottom), this uses either analysis or forecast fields from each weather model according to the labels on the above charts.

HYCOM, operated by FNMOC, is an ocean general circulation model used to study the ocean-atmosphere interactions [31]. Salinity is one (among several) of its output variables, provided at 1/12° horizontal resolution and 40 depth levels. HYCOM runs once a day at 12Z (yellow sectors in Fig. 14b) with 3-hourly output.

NAAPS is an aerosol model that produces 6-day forecasts of five species including gaseous sulfur dioxide (SO_2), particulate sulfate (SO_4), mineral dust, smoke/soot, and sea spray [32]. The operational NAAPS at FNMOC runs at a horizontal resolution of 1/3 degree with 35 vertical levels; an updated version in testing at NRL improves the horizontal resolution to ¼ degree and supports as many as 100 vertical levels. NAAPS is a post-processor running after NAVGEM. The operational NAAPS initializes the aerosol fields at time T – 6 hr.

NRLMRY is the lead developer of the Geolocated Information Processing System (GeoIPS) which is a generalized toolkit for processing and visualization of raw, processed, and retrieved satellite data, as well as numerical model outputs and other observation types. GeoIPS provides a common infrastructure and application programming interface to support rapid integration of new satellite data products into downstream workflows both human and automated. FNMOC uses GeoIPS for ingest and preparation of satellite data products.

4 APPROACH

The approach to achieve the stated objectives (Section 2) involves several tasks for each phase. The tasks formulated for each phase are based on our previous experience in developing the WindSat whitecap

retrieval algorithm (Section 3.1) and in modeling of the sea spray flux with the operational NAAPS (Section 3.2). These tasks are listed in the sections here as they were written in the NISE proposal.

The work in Phase 1 was performed solely by RSD, while RSD and NRLMRY worked in collaboration during Phase 2. This two-tier approach was devised for effective use of the team working time in FY21 and FY22.

4.1 Phase 1 tasks

The overall approach for the work planned for Phase 1 of this NISE project (FY21) was to modify the physical modeling of the WindSat whitecap retrieval algorithm and implement new code/software tailored for the specifications of the AMSR2 sensor.

The measure for success for Phase 1 was to deliver a working initial version of the whitecap retrieval algorithm with AMSR2 data as a proof-of-principle. This proof-of-principle version of the whitecap retrieval for AMSR2 was not expected to provide optimal performance. Rather, it would need further work by Code 7223 during Phase 2 to refine the modeling. However, it aimed to ensure that Code 7544 could start incorporating the algorithm in the operational NAAPS at Phase 2 beginning.

The elements necessary for passive remote sensing of W (Fig. 10) determined the 7 tasks implemented during Phase 1 (see the box top right in Fig. 10). Each task is associated with its corresponding element in the chart (red numbers in Fig. 10). The specific tasks visualized in Fig. 10 are as follows.

1) Atmospheric module: Adjust the parameterized atmospheric model for WindSat to AMSR2:
   - Run the atmospheric RTM for AMSR2 frequencies and EIAs;
   - Derive new parameterization coefficients based on atmospheric RTM results.
2) Roughness module: Adjust the parameterized roughness model for WindSat to AMSR2:
   - Update the specular emissivity model for AMSR2 frequencies and EIAs;
   - Derive new sea surface roughness parameterization coefficients for AMSR2 using an empirical roughness emissivity model.
3) Foam module: Adjust the parameterized foam emissivity model for WindSat to AMSR2:
   - Implement a new, improved parameterization of the existing RTM for foam emissivity and use it with AMSR2 frequencies and EIAs;
   - Optimize the performance of the parameterized foam emissivity model by tuning two foam parameters (foam layer thicknesses and foam void fraction) for each frequency-polarization channel;
   - Quantify the bias between the full RTM and the parameterized model for foam emissivity by assessing their differences over a range of observational (e.g., incidence angles) and environmental (e.g., sea surface temperature and salinity) conditions.
4) Simulate T_Bs with the AMSR2 forward model and compare to observed AMSR2 T_Bs for validation. Develop a first-order empirical correction to remove any biases.
5) Adapt the existing WindSat algorithm to retrieve first-cut EDRs from AMSR2 T_Bs to use as input for the whitecap retrievals.
6) Assemble the AMSR2 version of the whitecap retrieval algorithm.
7) Calculate first whitecap retrievals from AMSR2 data.

4.2 Phase 2 tasks

In the second phase (FY22), the goal was to demonstrate NRL readiness to provide initial air-sea interaction products using operational NAAPS. To achieve this goal, we needed to incorporate the whitecap retrieval algorithm in the operational NAAPS to provide sea spray production from AMSR2 in NRT.

The planned tasks were:

1) Set up near-real-time AMSR2 data flows, including monitoring of coverage and timeliness.
2) Develop and test a production system for the whitecap retrieval product using data inputs matching AMSR2 data already used operationally by FNMOC, with visualization and monitoring of the generated products using the GeoIPS framework.
3) Improve the AMSR2 whitecap retrievals by adjustments of atmosphere, roughness, and foam modules, as well as the AMSR2 EDRs serving as inputs. This work includes incorporating physically-based sea surface roughness modeling results for AMSR2 parameters.
4) Develop improved version of the whitecap retrieval software for NAAPS. Incorporate the improved whitecap retrieval software in NAAPS.
5) Monitor the whitecap retrieval by comparison with dynamic ocean surface fields used in existing NAAPS model. Compare satellite product to NAAPS model outputs at analysis time as well as 12, 24, 48, and 96-hour lead times.
6) Perform systematic verification of AMSR2 whitecap retrievals using existing in situ W data.
7) Optimize merging of satellite and dynamical whitecap fraction estimates for NAAPS forecasts.
8) Characterize and document first sea spray production from NAAPS as a new aerosol product.

5 RESULTS

5.1 Phase 1

In Phase 1, we completed all 7 tasks as planned. Below, the results on these 7 tasks are presented in three groups: the forward model for whitecap retrievals (tasks 1-4); the AMSR2 retrievals as input to the models in the whitecap retrieval algorithm (tasks 5-6); and retrieval of whitecap fraction (task 7).

5.1.1 Forward model for whitecap retrievals

The results presented here are for tasks 1-4 (visualized in Fig. 10 with red numbers in green boxes). The modeling modules for these tasks are described in Section 3.1.2.

The atmospheric module computes the atmospheric parameters t, T_{BU}, and T_{BD}. As outlined in Section 3.1.2, we started with a physical atmospheric RTM, which simulates vertically-resolved profiles of t, T_{BU}, and T_{BD}. We used a monochromatic RTM called MonoRTM (v. 5.4, Atmospheric and Environmental Research, Inc.). Because the microwave frequencies (Table 1) cannot resolve layers in the atmosphere, we must apply the one-layer isotropic atmosphere approximation representing the full atmospheric column as one layer. We thus integrated the atmospheric profiles to obtain columnar values of t, T_{BU}, and T_{BD} for each AMSR2 frequency.

The resulting physical data compiled a database of the atmospheric variables t, T_{BU}, and T_{BD}. We used this database to make regressions for t, T_{BU}, and T_{BD} thus ensure their fast, NRT computation (Section 3.1.2). The regressions are functions of T_s, V, L and EIA, and are derived separately for each AMSR2 frequency (Table 1).

The roughness-only module computes term e_r in (1). The 2-scale model is run for all AMSR2 frequencies to calculate the foam-free roughness term for a range of wind speeds, SSTs, and EIAs. This

database of physical values is then used to parameterize the roughness-only term as a function of wind, SST, and EIAs. A table of roughness-only emissivity coefficients is saved and is later used as an input to the forward model for the whitecap retrievals.

Because of the lengthy computation of the physical values, in Phase 1 we delivered an effective reflectivity of the sea surface representing only the large-scale waves. This ensured good performance of the roughness-only module for the proof-of-principle version of the whitecap algorithm.

The foam emissivity module computes the 100% foam-covered emissivity E_f in (1). As noted in Section 3.1.2, the upper void fraction limit can serve as a tuning parameter due to the foam emissivity sensitivity to its values for different frequencies. This is exactly what we changed in the foam emissivity RTM adapted for AMSR2 during NISE Phase 1. The foam properties specific for frequency and polarization are given in Table 2. The tuned values in Table 2 are close in magnitude, but the frequency dependence of the foam emissivity E_f (shown in Fig. 15 for H polarization) for fixed and tuned foam properties shows the difference is notable.

Table 2 — Foam properties (foam layer thickness d and upper limit of the foam void fraction v_{af}) tuned for the AMSR2 frequencies F (GHz) and polarizations (H and V). The band for each F is given in parentheses.

***F* (GHz)**	***d* (cm)**	**v_{af} for V**	**v_{af} for H**
6.925 (C)	0.6	0.95	0.96
7.3 (C)	0.6	0.95	0.96
10.65 (X)	0.4	0.95	0.964
18.7 (K)	0.2	0.96	0.968
23.8 (K)	0.15	0.965	0.97
36.5 (Ka)	0.1	0.97	0.97
89.0 (W)	0.1	0.97	0.98

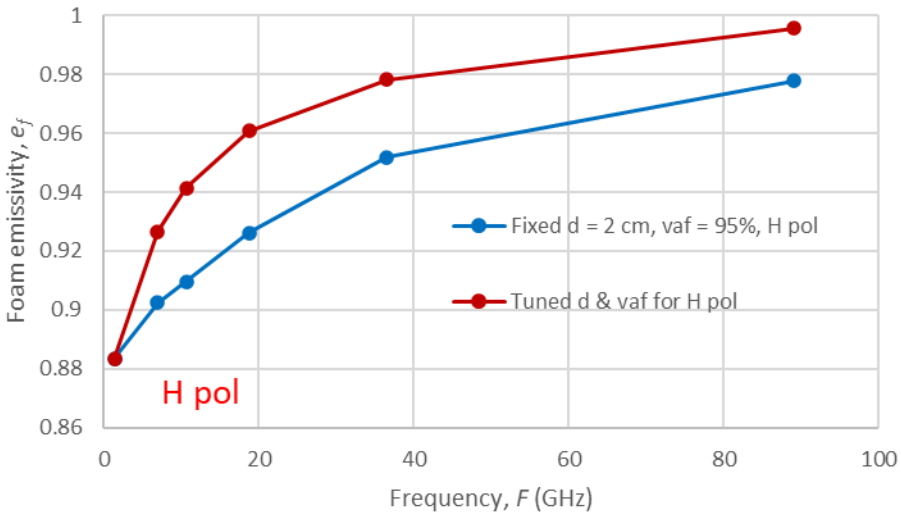

Fig. 15 — Foam emissivity (for H polarization) as a function of frequency for foam properties with fixed values (blue line) and tuned values (red line).

We validated the effect of tuned foam properties (versus fixed) with independent RTM and AMSR2 data. We used a community code for ocean-atmosphere RTM to model T_B at the TOA, once with foam properties at fixed values and then for tuned foam properties. We compared the simulated T_B with T_B observations from AMSR2 and found that the difference between modeled and observed T_Bs decreased by 10% to 50% when using the tuned foam properties for E_f instead of foam properties with fixed values.

The foam emissivity RTM was used to calculate physical values for E_f for all AMSR2 frequencies and the EIA range (Table 1) covered with a step of 0.1°. The parameterized model for E_f uses the Fresnel formula to obtain reflectivity (and emissivity) at the foam upper boundary for each AMSR2 frequency and polarization and fixed EIA = 55°. Corrections derived from the physical values are added to these "Fresnel" values to minimize the difference between the foam emissivities calculated with the physical and parameterized models.

With the modules for the atmosphere, roughness-only, and foam emissivity, the forward model for the whitecap algorithm was complete. Its implementation was tested by running it with input variables (U, V, L, T_s, and S) from Mercator Ocean reanalysis (GLOBAL_ANALYSIS_FORECAST_PHY_001_024 distributed by the Copernicus Marine Service, [33]) and ERA-Interim (ECMWF Re-Analysis, v. 4).

5.1.2 AMSR2 Retrievals

Our experience with the WindSat whitecap algorithm showed that the noise of the W retrievals is minimal when using both the WindSat observed T_B and the WindSat EDRs (Section 3.1.2). Therefore, we need AMSR2 EDR retrievals for use as input parameters driving the modelling modules in the whitecap algorithm. As described in Section 3.1.3, to retrieve AMSR2 state vector (U_{10}, V, L, T_s), we need to develop a forward model, which we can use to produce AMSR2 EDRs using AMSR2 T_B observations (not shown in Fig. 10).

We thus developed a new retrieval algorithm to simultaneously retrieve T_s, U_{10}, V, L from AMSR2 observations of T_B. Building on the WindSat experience, the AMSR2 retrieval algorithm employs the nonlinear optimization method we developed for WindSat (Section 3.1.3). The AMSR2 EDR retrievals use the following elements:

1) Observed T_B values: We use the Japan Aerospace Exploration Agency (JAXA) AMSR2 L1R data. These were ingested with an offline code. Only the lowest (coarse) resolution of AMSR2 data (C-band resolution) was used for the initial retrievals. This enabled retrieval of all four EDRs including SST. Quality controls for rain, sea ice and land were done using Remote Sensing System (RSS) data.
2) Forward model: The forward model for the AMSR2 retrievals is consistent with the forward model used for the whitecap retrievals except that the sea emissivity is our implementation of the empirical emissivity (roughness + foam) model described in [34].
3) Inputs forcing the AMSR2 forward model: These come from different sources. An initial estimate for the SST is taken from collocated Mercator data with two degrees of random noise added to simulate the error in an NWP forecast. The salinity and wind direction are taken from Mercator and ERA-Interim, respectively. AMSR2 and the external model data (987,235 data sets) were matched up in time and space for 3 days (5, 15, and 25) in 4 seasons (January, April, July, and October) in 2016. The collocation was done with interpolation to the nearest neighbor.
4) Empirical offsets: We need these to better match the WindSat forward model to the AMSR2 T_B. They are based on our initial calibration work.

We validated the AMSR2 EDR retrievals by comparing them to geophysical variables from the ERA-Interim model. Density plots in Fig. 16 show NRL retrievals of U_{10} (left panel) and T_s (right panel) versus model U_{10} and T_s values.

The mean bias of NRL U_{10} retrieval versus ERA-Interim is 0.1 m s^{-1} and the standard deviation is 1.46 m s^{-1}. For the SST retrievals, these statistics are bias of 0.09 °C and standard deviation of 0.83 °C. For V, these are 1.28 and 2.74 mm, respectively. These results for the initial version of the algorithm verify that our retrieval methods will produce the retrieval performance needed to support whitecap retrievals.

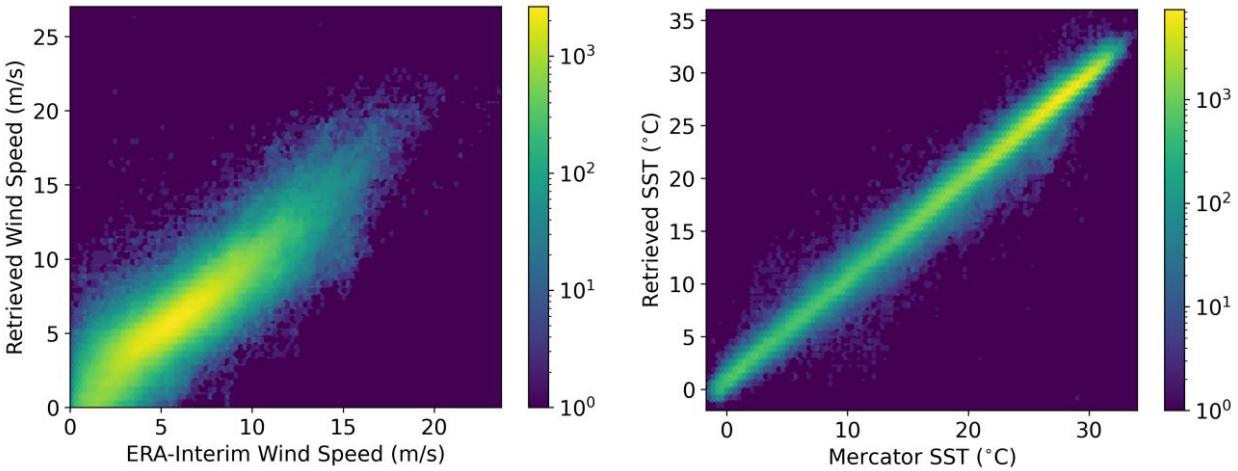

Fig. 16 —One-to-one comparison of AMSR2 retrievals and modeled data for wind speed U_{10} and SST T_S. The color bar shows number of data points.

Having the AMSR2 EDR retrievals to use as input to the forward model, we next implemented the whitecap algorithm. For this we use the (3), but this time the T_B^{TOA} data are from AMSR2, T_{Br}^{TOA} comes from the roughness-only module, T_{Bf} is from the foam module, and factor A uses the atmospheric parameters obtained with the atmospheric module; Fig. 17 visualizes the AMSR2 version of the whitecap retrieval algorithm.

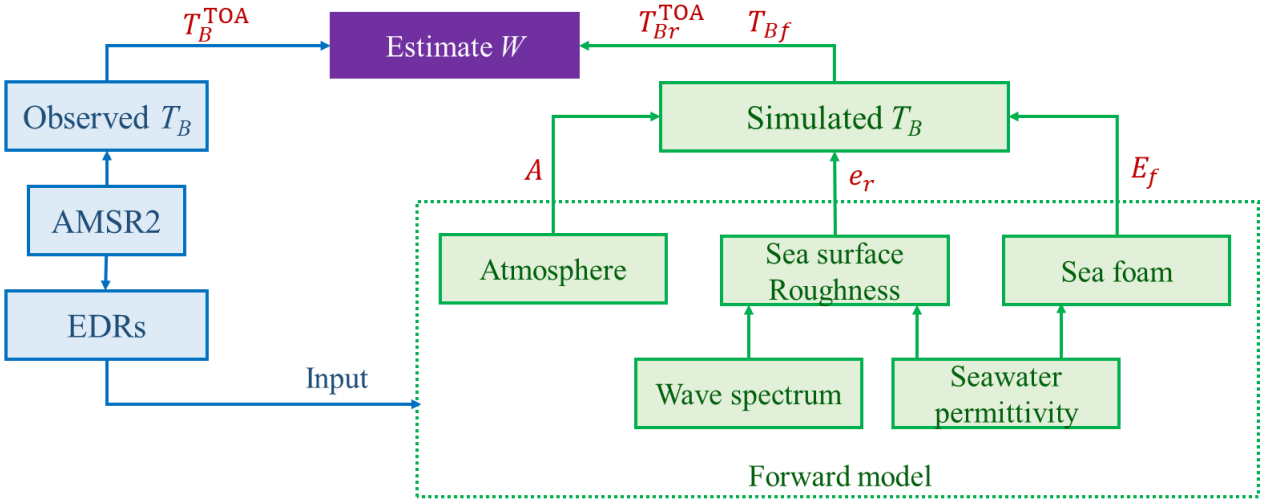

Fig. 17 — Flow chart for the whitecap retrieval algorithm visualizes the modules providing the quantities in (3).

5.1.3 Whitecap retrievals from AMSR2

With the whitecap retrieval algorithm, we retrieve W from the AMSR2 T_B observations for the 987,235 data points (Fig. 18). The W retrievals from Fig. 18 are shown in Fig. 19 binned by wind speed (with bins of 1 m s^{-1}) in order to compare their wind speed trends with the in situ data and the $W(U_{10})$ parametrization from Fig. 4. The standard deviation of the binned data points, averaged over the wind speed range, is given for each frequency. The standard deviation shows the spread of the AMSR2 W retrievals. This spread includes both the modeling errors of the whitecap algorithm and the natural variability of W during 2016 over the globe.

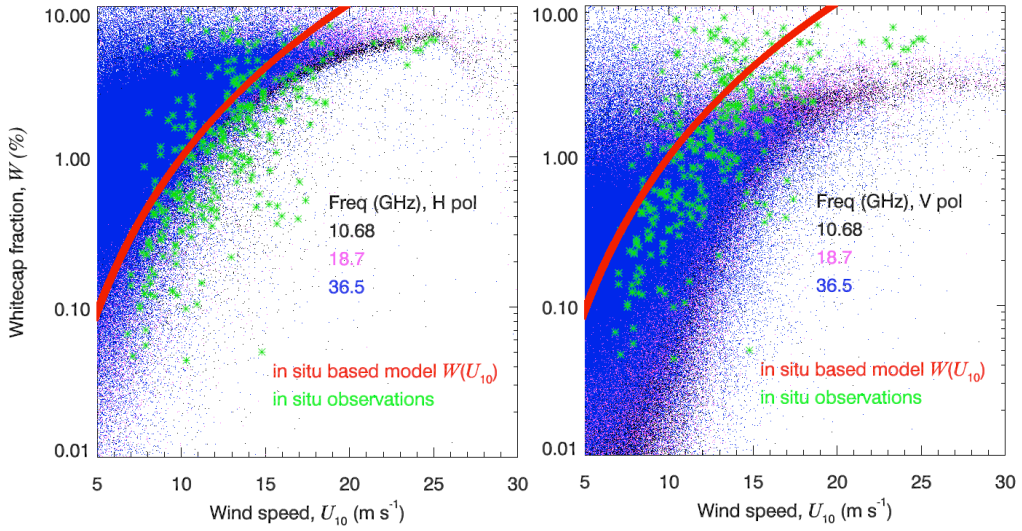

Fig. 18 — AMSR2 retrievals of whitecap fraction as a function of wind speed for different frequencies (black, magenta, blues): a) for H polarization; b) for V polarization. The same in situ data and $W(U_{10})$ parametrization from Fig. 4 are shown for reference.

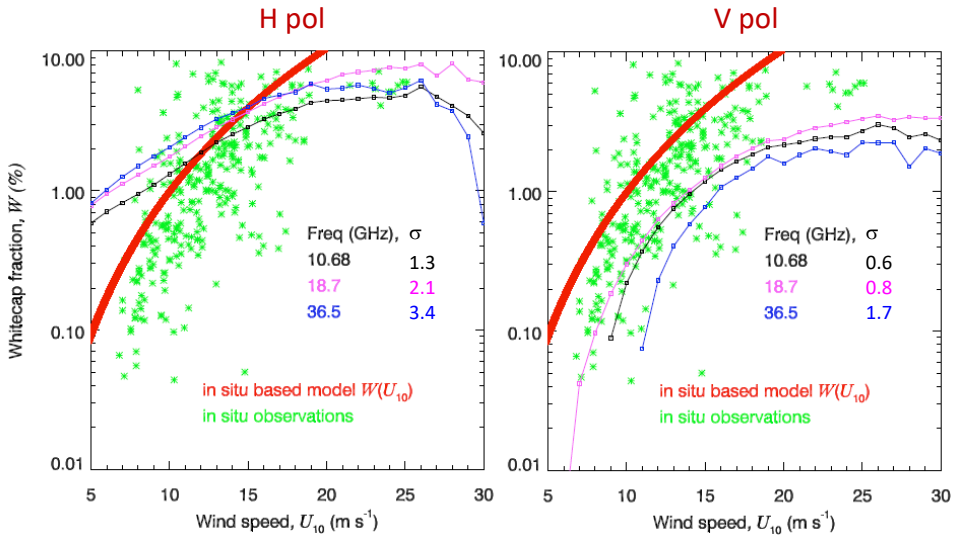

Fig. 19 — AMSR2 retrievals of whitecap fraction as a function of wind speed for different frequencies binned by wind speed (black, magenta, blues): a) for H polarization; b) for V polarization. The same in situ data and $W(U_{10})$ parametrization from Fig. 4 are shown for reference.

The results in Fig. 19 show that the initial version of the AMSR2 whitecap retrieval algorithm produces values that are order-of-magnitude comparable to the in situ W observations. The retrievals for V pol track well with the in situ W data at low wind speeds, while the retrievals for H pol track well with the in situ W data at high wind speeds. The comparison for H pol to the $W(U_{10})$ parameterization suggests that the overestimation for high winds is now removed; for V pol, the trend with the wind is too low for $U_{10} > 12–15$ m s^{-1}. However, at low winds, the W retrievals for H pol are biased high compared to $W(U_{10})$. One possible way to improve this is the modification of the roughness-only module (Section 4.2).

5.2 Phase 2

5.2.1 Near-real-time data input for the whitecap algorithm

The Phase 1 work on the whitecap algorithm used an archived (static) data from AMSR2 with time-space matchups of METOC variables (Section 5.1). To transfer and incorporate the whitecap algorithm code in the operational NAAPS, an NRT flow of AMSR2 data is required as well as data input/output formats consistent with those used in the operational NAAPS. These two requirements shaped the initial work on setting up a production system for interfacing the whitecap algorithm to the operational NAAPS using both archived and NRT AMSR2 data.

We work with AMSR2 L1R data to leverage the current use of these data in NAVO for sea ice retrievals. It is also important that the L1R T_B data are resampled to a common footprint (Appendix B). The AMSR2 files have two sets of latitude/longitude fields for 89 GHz denoted '89A' and '89B.' The common footprint resampling for L1R data is done to the 89A locations; thus, we use only those T_B data. We use archived AMSR2 L1R data from JAXA. NRT feed of AMSR2 data is from NOAA Production Distribution and Access (PDA).

We also use global model outputs (gridded fields) for additional METOC data necessary as inputs to the whitecap algorithm (Section 3.3); these model output data are listed in Table 3. We use the "surface" model fields from the models, which are the lowest atmospheric layer from NAVGEM and NAAPS and the uppermost ocean layer from HYCOM.

The model outputs are both archived and NRT data. NAAPS provides archived data. The NRT data from Navy models come from Global Ocean Data Assimilation Experiment (GODAE). GODAE files are retrieved multiple times per day from FNMOC via the Come and Get It Processing System (CAGIPS). For NRT product, we use both analysis and forecast fields of the models to ensure timely production of retrieval products (see Fig. 14). Because of the operational duty cycle of the different NWP models, the model data range from analyzed atmosphere and ocean data for times near 12Z to 6-hour forecasts from NAVGEM and 18-hour forecasts from HYCOM for satellite observations near 06Z. The impact of the use of forecast fields is expected to be small.

With the data sources determined, we proceeded to creating value-added AMSR2 products with Navy model METOC fields (Table 3) resampled onto the AMSR2 grid. The METOC fields are matched (sampled) spatially to AMSR2 L1R data by taking the nearest neighbor. In time, AMSR2 data are matched to NAVGEM at previous 00Z or 12Z watch (Fig. 14a) and the data point with the smallest time difference is selected. For HYCOM, AMSR2 data are matched to current or previous day (Fig. 14b); again, data point with the smallest time difference is selected. The combined AMSR2 and METOC fields are saved in NetCDF files. RSD used a prototype of these NetCDF files to work on improving the whitecap retrieval algorithm and interfacing it to NAAPS.

Table 3 —METOC data from global model outputs matched in time and space with AMSR2 data.

Field	Name in NetCDF file	Source	Units	Resolution	Vertical
Air Temperature	air_temp	NAVGEM	K	0.5°	1013.2 hPa
Dewpoint Depression	dwpt_dprs	NAVGEM	K	0.5°	surface
Relative Humidity	rltv_hum	NAVGEM	%	0.5°	1000 hPa
Meridional wind	wnd_vcmp	NAVGEM	m s^{-1}	0.5°	1013.2 hPa
Zonal Wind	wnd_ucmp	NAVGEM	m s^{-1}	0.5°	1013.2 hPa
Land/Sea surface temp	grnd_sea_temp	NAVGEM/ HYCOM	K	0.5°	Surface
Salinity	sal	HYCOM	kg/kg	0.125°	Surface
Sea Salt Concentration	aero_concen_sa	NAAPS	mg m^{-3}	0.5°	Surface

5.2.2 Improved algorithms for AMSR2 EDRs and whitecap retrievals

To facilitate rapid development during Phase 1, the whitecap retrieval was implemented in a separate code (Section 5.1.3) from the code that retrieved the other EDRs (Section 5.1.2). The initial step of the Phase 2 development combined the two algorithms into a single code (i.e., the codes for the green and brown boxes in Fig. 10 were put together) to simplify deployment and reduce input and output overhead. A code was added to ingest the new inputs from the NetCDF files provided by the production system (Section 5.2.1). With this, the updated code can now be used with both NRT and archive AMSR2 L1R data combined with NWP forecast from NAVGEM and HYCOM (Table 3) for initialization when they are available in the NRT data.

The Phase 1 retrievals use the low resolution AMSR2 L1R data (the resolution of the 6.925 GHz channels). The new code is now implemented in three stages. The first stage uses the AMSR2 channels up to 36.5 GHz to retrieve the most accurate SST. The second stage uses the first stage SST and the T_B values of 10.65-36.5 GHz channels at the 10.65 GHz resolution. The third stage retrieves the whitecap fraction at the 10.65 GHz resolution. This implementation retrieves the most accurate SST while also retrieving the whitecap fraction with improved resolution.

The forward model for the AMSR2 geophysical retrievals was also improved. The permittivity model was updated to the model from [35] to improve the accuracy of the sea emissivity in the forward model. Calculation of both the sea surface emissivity and reflectivity was reimplemented to provide a continuous Jacobian of the forward model over the full ranges of the retrieved EDRs. New T_B calibration coefficients were derived to better match the forward model to the AMSR2 T_B values to account for differences between AMSR2 and WindSat sensor calibration. The new calibration offsets were derived using a collocated dataset from the ERA5 NWP model (the fifth generation ECMWF atmospheric reanalysis of the global climate covering the period from January 1950 to present) and retrieval atmospheric parameters from RSS.

Retrieval accuracy is degraded when the T_B values are affected by radio frequency interference (RFI), rain, sea ice, land contamination and sun glare. Quality control flagging has been added to the code to identify retrievals that are likely affected by any of these effects. Land contamination occurs when the T_B

field-of-view partly intersects with a coastline and is flagged using a threshold of the land fraction as given in the AMSR2 L1R data. Retrievals are flagged for sun glare when the angle between the specular reflection of the solar energy from the ocean surface and the AMSR2 look direction is less than 25°. Retrievals are flagged for rain whenever the retrieved columnar cloud liquid water is greater than 0.2 mm. Additionally, we have implemented flagging based on threshold for the χ^2 statistic of the difference between the forward model T_B using the retrieved EDRs and the observed AMSR2 T_B (Section 3.1.3). This effectively screens out RFI, improves flagging for sea ice, and flags spurious T_B values.

For the whitecap algorithm, two new outputs were added to the code. One is a "best value" of whitecap fraction retrievals, which combines *W* retrievals at different frequencies and polarizations (Section 3.1.2) in one value. While the frequency-dependent *W* values are useful in interpreting different physical processes at the air-sea interface, most oceanographic applications require one *W* value. The best *W* value gives this common, effective *W* retrieval. Different methods can be used for combining the *W* retrievals at different frequencies and polarization. In this project, the best *W* value is the average of all *W* retrievals at different frequencies and polarizations. (Choosing the most suitable combining method to get best *W* values is beyond the scope of this project.) We also added in the whitecap algorithm a computation of the total sea spray flux using (8) with the best *W* value (Section 3.2.1). Finally, a new code was written to save updated whitecap algorithm output in a NetCDF file. The full code was then provided to NRLMRY for further developing and testing the production system (described in Section 5.2.4).

5.2.3 Verification of the updated whitecap retrievals

The conventional way of verifying/validating satellite retrievals of geophysical variables is to make 1-to-1 (1:1) comparison with space-time matched in situ *W* data. Usually time-averaged in situ data are used to compare meaningfully to the satellite data, which are space-averaged over the footprint of the satellite-borne sensor. We used in situ *W* data to verify the results of the improved AMSR2 retrievals (Section 5.2.2).

Major problem with in situ *W* measurements is underreporting of their times and locations (as latitude/longitude pairs). We obtained an in situ dataset for 2017 with times and locations after contacting the authors [8], hereafter referred to as B17 dataset. We retrieved *W* from AMSR2 observations for the B17 dataset period and matched them in time and space with the in situ *W* values. The temporal matching criterion was to find all AMSR2 observations within ± 3 hr around the time of each in situ data point; the 3-hr period was chosen to increase the number of in situ-satellite pairs. Then spatial matching criterion was applied to those temporal matches to find and take the nearest AMSR2 data point that is found within 60 km around each in situ location.

After screening out flagged AMSR2 data, there are 21 collocations with the B17 measurements, all of them within 6 km distance. Both the 1:1 comparison and the wind speed dependence of these matched-up data produced poor (noise-like) results. Figure 20 demonstrates this; the color in the plots is the magnitude of the time difference in hours. Figure 20a shows that the B17 measured *W* versus the B17 wind speed does not show a clear trend. Figure 20b shows that the B17 versus AMSR2 wind speeds are at least in the same range, but not well correlated within that range. The 1:1 comparison of B17 *W* to AMSR2 best *W* values is just as noisy as the wind speed comparison in Fig. 20b. Finally, Fig. 20c shows that the AMSR2-retrieved best *W* values versus wind speed look reasonable.

To identify the reason(s) for such poor comparison, we made similar match-up of *W* retrievals from WindSat to the same *W* from the B17 dataset. We found similar number of matched in situ−satellite pairs with similarly poor results when plotting the 1:1 comparison and the wind speed dependence. Because the satellite *W* retrievals from WindSat and AMSR2 are independent, such results suggest that there are large uncertainties in the in situ *W* dataset or that the in situ measurements are not representative of the spatially-averaged satellite views.

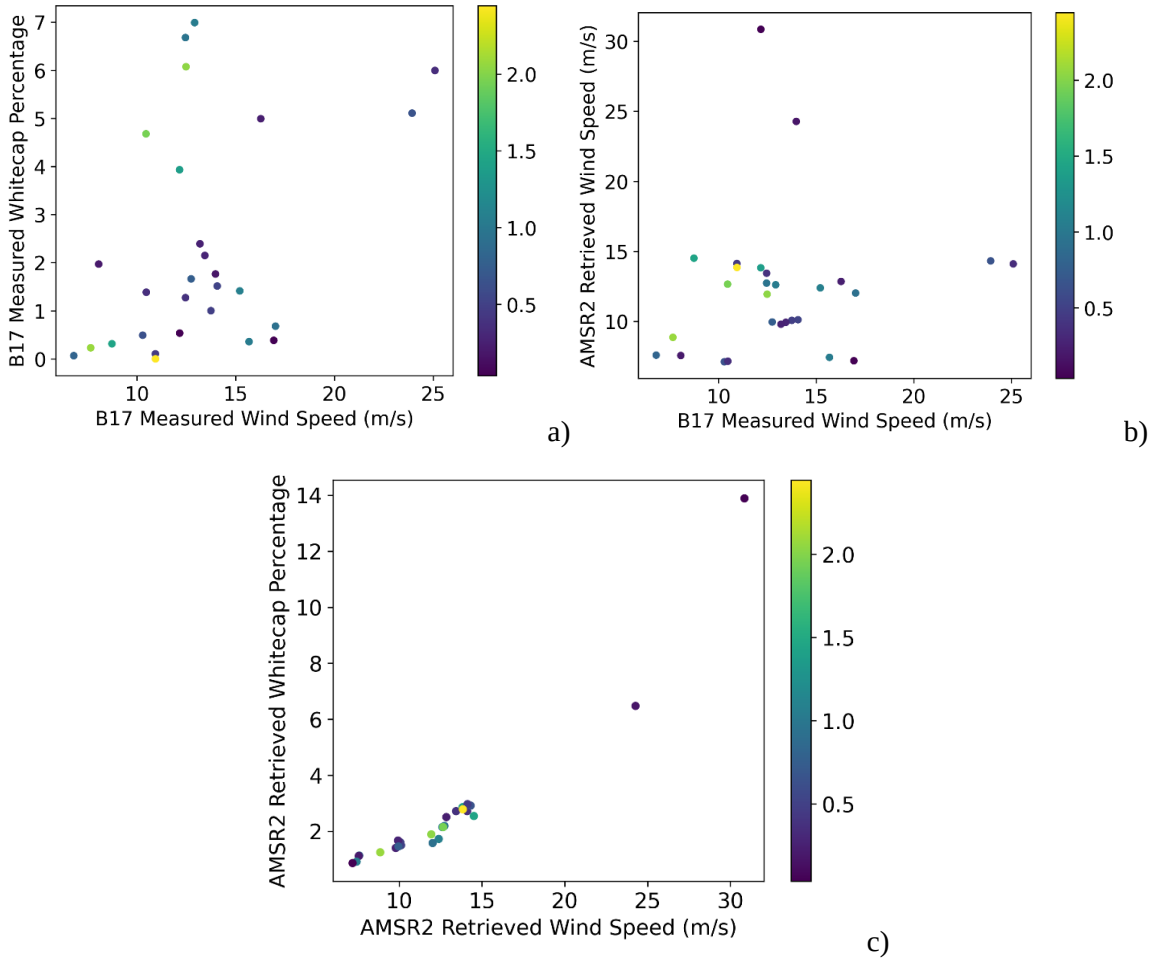

Fig. 20 — Comparison of satellite and in situ data for whitecap fraction W and wind speed U_{10}: a) Wind speed dependence of W from in situ data; b) 1:1 comparison of AMSR2 retrievals of U_{10} and in situ measurements of U_{10}I; c) Wind speed dependence of W from AMSR2. The color in all panels is the magnitude of the time difference (in hours) between satellite and in situ data points.

These results make two points. First, they demonstrate the need for better ways to measure whitecap fraction than using in situ measurements and $W(U_{10})$ parameterizations based on them. Second, these results confirm the long-standing difficulty we have been having when validating the satellite W retrievals with in situ W data. These results thus justify our efforts to look for what we call indirect validation involving not directly in situ W data but rather variables derived using W and matched to independent measurements of these variables. Using AOD from ENAAPS or the operational NAAPS are apt examples for such validation.

5.2.4 Near-real-time processing of the whitecap retrieval

With the concept for a dynamic data flow established (Section 5.2.1) and tested with the updated whitecap algorithm (Section 5.2.2), NRLMRY proceeded with the implementation of a complete integrated workflow to NRT download, ingest, and processing of the AMSR2 whitecap retrieval. Figure 21 shows the structure of this workflow, which was constructed using the Cylc workflow engine (https://cylc.github.io/). Cylc allows the user to specify the prerequisites of each task, so that tasks can run as soon as their prerequisites are met rather than at specified wall times (though clock control of tasks is also possible).

Every hour, the Cylc suite checks for newly arrived AMSR L1R files on the NOAA PDA download servers. If new files are available, these are downloaded, and processing is begun, first adding in the model meteorological fields, and then running the whitecap retrieval software.

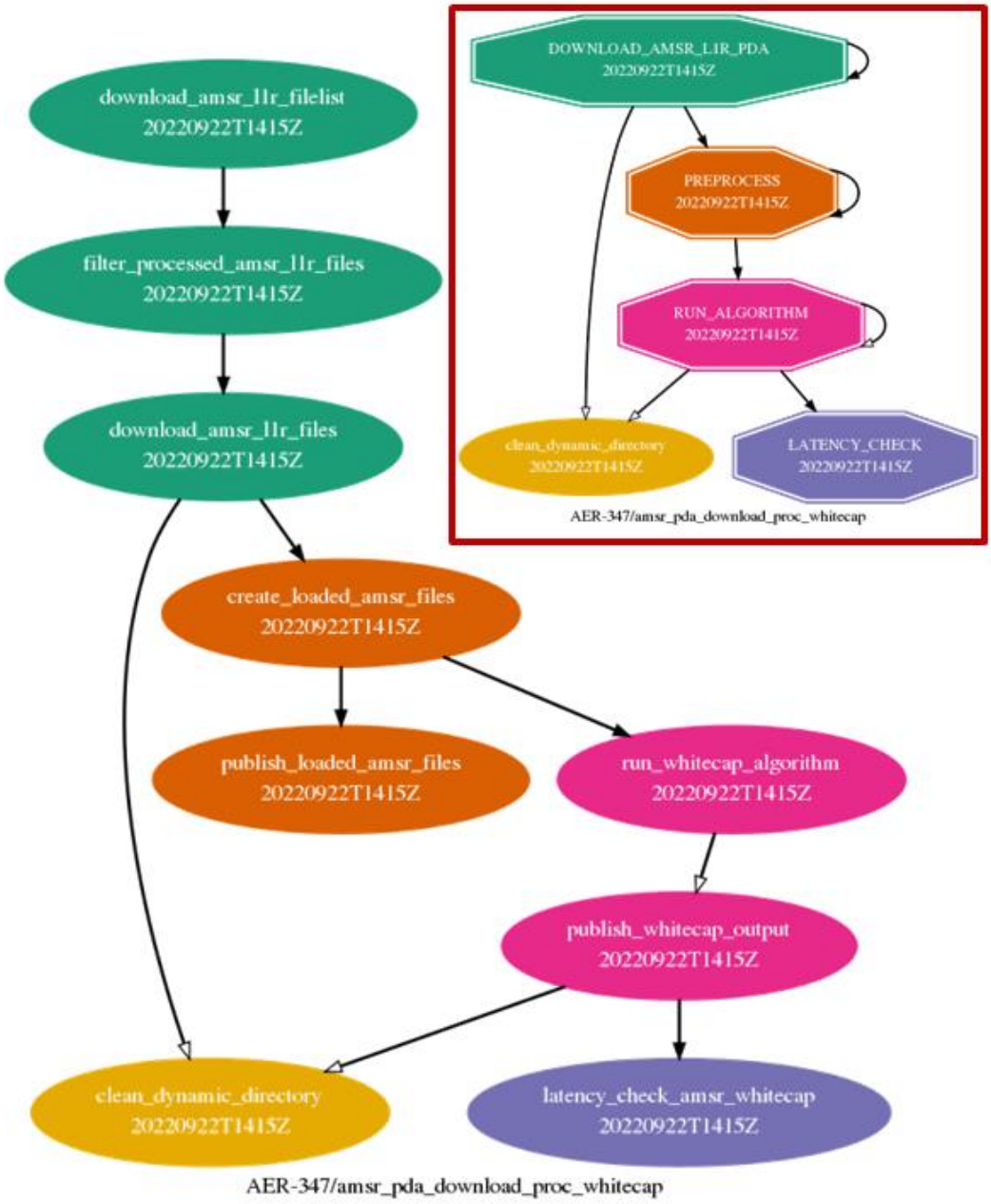

Fig. 21 — Dependency graph shows tasks and dependencies for the Cylc workflow to manage near-real-time download, ingest, and processing of whitecap retrieval products developed under this project. The graph shows the tasks undertaken at each cycle point, with arrows indicating sequential tasks. The inset (upper right) shows the tasks grouped by families.

The latency of AMSR2 L0 and L1 data processing and delivery via NOAA PDA and downloading to NRLMRY is typically 121-257 minutes (133 minutes on average) from satellite overpass time to when AMSR L1R products (3.3 GB per day) are available for download. Addition of the meteorological fields

only takes <1-2 minutes, but the dependency on waiting for meteorology files on GODAE typically results in a 123-855 minute latency with respect to the granule start time (377 minutes on average). The whitecap retrieval algorithm itself takes on average 7 minutes per file when running NRT. The total latency of retrievals available for use in downstream systems is typically 131-836 minutes from the satellite overpass time (405 minutes on average). Figure 22 shows a time series depicting the latencies of AMSR2 data within a granule from the NRT processing suite on NRLMRY's system.

In testing of the NRT processing, we found that latency of the model forecast data was sometimes a limiting factor. A significant part of this latency was associated with delivery of model forecast fields from FNMOC to the public GODAE servers; this latency would not apply once the product was transitioned to operations. However, for applications requiring the minimum latency at all times, this could be mitigated by using older model fields (e.g., 24-hour forecasts instead of 12-hour). Impacts of those decisions on retrieval quality would need to be tested.

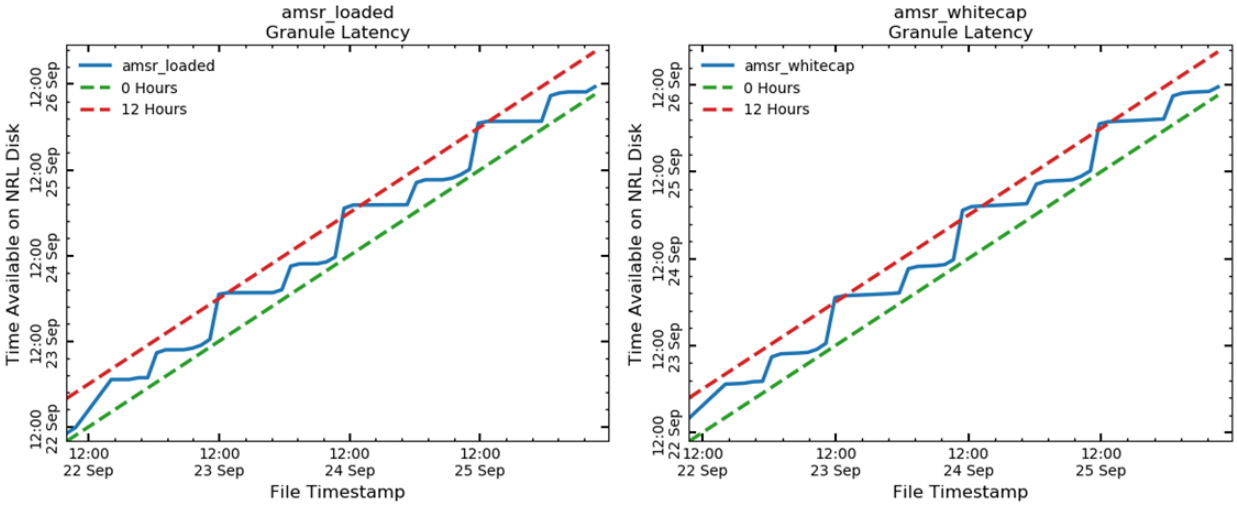

Fig. 22 — Time series of the file latency of AMSR loaded files (AMSR L1B files with meteorology fields added from GODAE), and AMSR whitecap files. The x-axis represents the start time of the granule, and the y-axis shows the time when the file was created on NRLMRY systems. The large latency for both products is due to the latency of meteorology files from GODAE.

5.2.5 Visualization of sea state retrievals using GeoIPS

Integrating the retrieval products into GeoIPS required a new plugin repository, titled whitecaps_retrieval and stored in NRL's GeoIPS GitHub project (GEOIPS (navy.mil)). The first addition to this repository was a new AMSR2 whitecap reader for the files. This task was relatively straight forward because the files were already in NetCDF self-documenting format. Within this reader, filters for QC flags and missing value replacements are applied.

Once a reader was constructed, product and input configuration files were generated to produce the new products from the dataset's fields. One file, called a product input file, specifies each new product name and its required variable(s). The other configuration files (one for each new product) determine the product's naming convention, interpolation method, and the color map applied in the image, in addition to other configurable parameters. Together, these files inform GeoIPS how to spatially process and visualize the data.

While GeoIPS includes default colormaps that can be applied to new product imagery, these unique products required new colormap options. Additional user colormap options were created for each

quantitative output. These new colormap functions also allow for users to modify colormap bounds and to change the base color scale.

Lastly, the new whitecaps retrieval plugin was constructed with config-based processing, a new GeoIPS feature, in mind. This processing method consolidates many of the configurable elements mentioned above into a single file that is passed through the GeoIPS command line interface. The input file produced in this case contained the requested sectors, the five products desired from the whitecap dataset—water vapor, cloud water, 10 GHz wind speed, whitecap fraction *W*, and sea spray flux—and a background image for context using RGB visible reflectance from the Advanced Himawari Imager (https://www.data.jma.go.jp/mscweb/en/himawari89/space_segment/spsg_ahi.html). This type of overlay product leverages a new capability of GeoIPS through the new config-based processing feature.

Figures 23 and 24 show visualization of AMSR2 sea state retrievals including sea spray flux for two example domains. The first domain (Figure 23) is an open ocean area of the north Atlantic chosen for its dynamic and variable atmospheric and oceanic conditions. The second domain (Figure 24) is centered on the recent TC Fiona and includes comparison with a standard IR satellite product used to assist forecasters with characterizing and predicting tropical storm behavior. These domains were generated by NRL's TCWeb application (https://www.nrlmry.navy.mil/TC.html). The information provided by the new retrieval product is both novel and complementary to the existing satellite data products in the TCWeb suite.

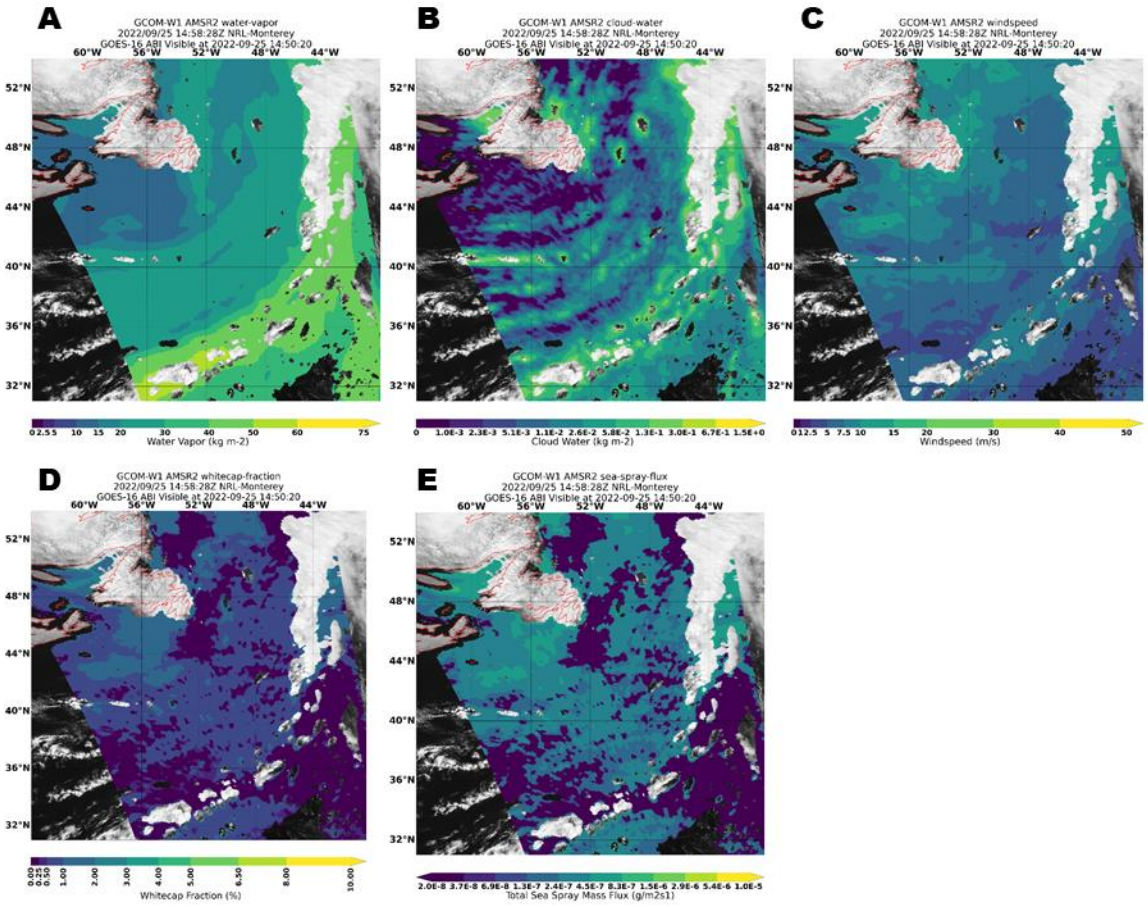

Fig. 23 — Visualization of the new AMSR2 retrieval products using GeoIPS. Each map shows a different retrieved quantity from the new algorithm: (a) water vapor; (b) cloud water; (c) 10 GHz wind speed; (d) whitecap fraction *W*; and (e) sea spray flux.

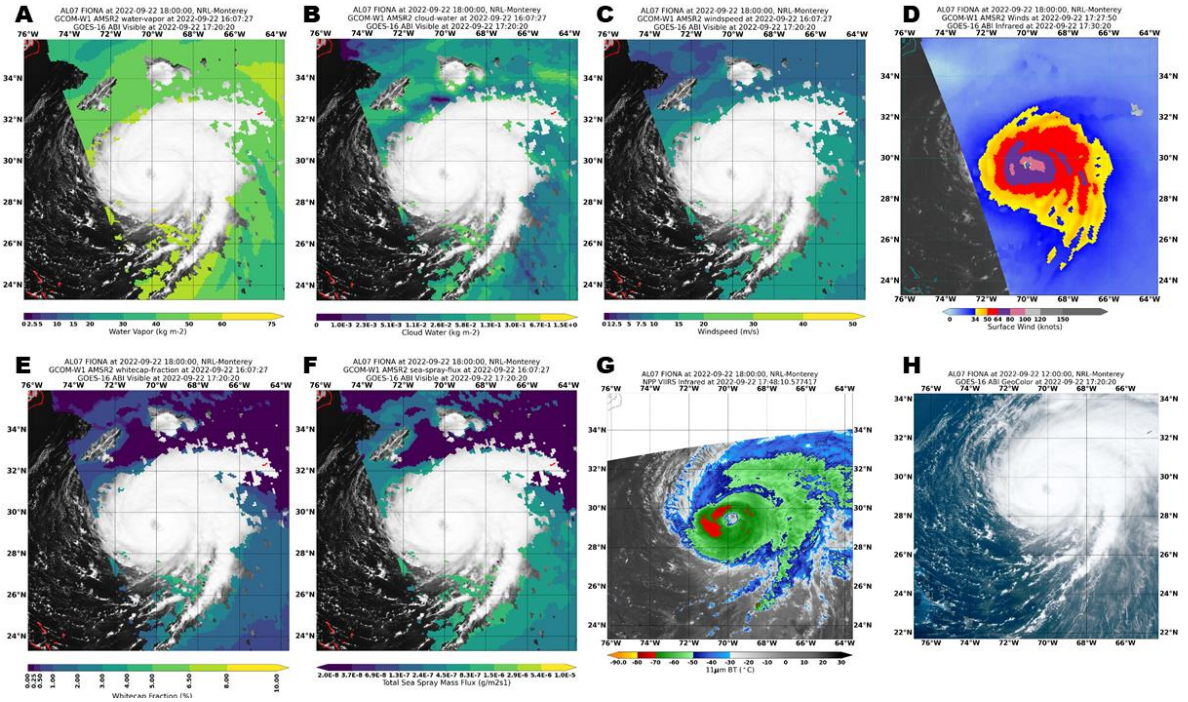

Fig. 24 — Demonstration of the new AMSR2 retrieval products for a domain centered on TC Fiona. (a-c) and (e-f) are as in Fig. 23. Additional products shown are from the NRL TCWeb standard processing which tracks tropical cyclone activity and supplies a wide range of satellite and model data products for forecasters, including (d) AMSR2 winds retrieved by the All-Weather Wind Speed algorithm developed at NOAA; (g) IR brightness temperature indicating the approximate cloud top heights in the TC system; and (h) RGB imagery from GOES-16 Advanced Baseline Imager processed using the GeoColor algorithm from Colorado State University.

5.2.6 Sea spray production from NAAPS

The presentation of the sea spray production with (8) and different *W* parameterizations (Section 3.2) has been used to modify the operational NAAPS code to include different cases. These are referred to as "Monahan" for the combination of (8) and (6), the scheme used by the operational NAAPS; "Salisbury" for combining (8) and (11), used by ENAAPS; "Brumer" for (8) and (9) combination; and "Albert" for (8) combined with (12). All these sea spray flux parameterizations are now available in the operational NAAPS. Figure 25 shows the AOD and vertical profile of the sea salt aerosol based on NAAPS simulations from a cold start (no atmospheric aerosols at initial time) for each of these parameterizations.

What can be seen in Fig. 25 is that the horizontal pattern of sea salt aerosol is largely driven by recent variation in wind speed, and the vertical profile reflects the mechanism used to represent sea salt lifting in NAAPS. Lifted sea spray aerosol is partitioned into the bottom two layers of the NAAPS model and then the turbulent mixing and resolved advection in the model carry some to higher altitudes, while much of the lifted salt is immediately re-deposited. However, the parameterization of *W* can be seen to affect the magnitude of sea salt global distribution and to alter the spatial patterns observed around high wind areas such as the Gulf of Alaska.

An additional comparison was performed to examine how the distribution of *W* retrieved from AMSR2 compared to what is obtained via parameterization in NAAPS using NAVGEM surface winds, and alternatively what would be estimated using the parameterizations driven by retrieved surface winds from AMSR2. These results are shown in Fig. 26.

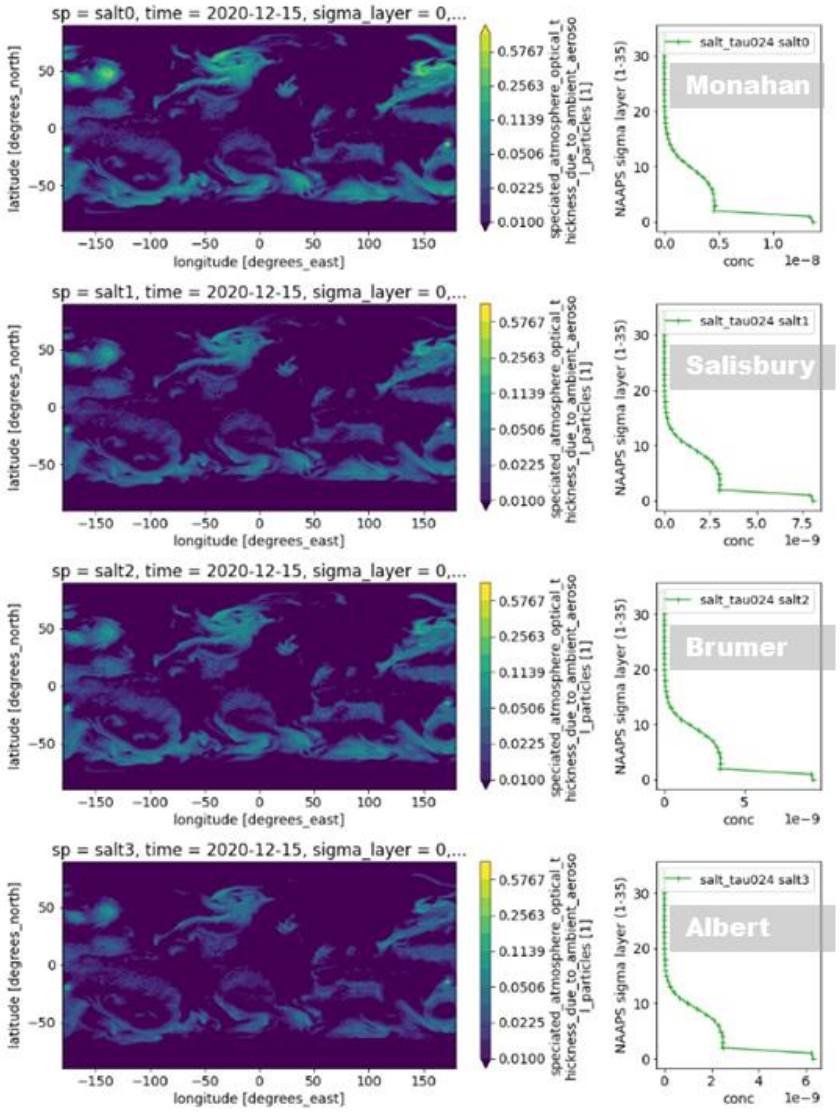

Fig. 25 — Aerosol optical depth from sea salt (left) and mean vertical profiles of sea salt (right) from NAAPS runs using four different parameterizations to estimate whitecap fraction *W*. Refer to the text for the labels Monahan, Salisbury, Brumer, and Albert.

Figure 26 shows important differences between the parameterizations, with the Monahan formulation used in the current operational NAAPS yielding significantly higher estimates of *W* compared with all other methods. Differences between AMSR2 retrieved surface winds and NAVGEM also manifest in different estimates of *W*. The AMSR2 retrieved distribution of *W* most closely matches the Albert or Brumer parameterizations.

As noted in Section 3.2.1, AMSR2 retrievals could be directly used in the operational NAAPS model in place of the parameterized whitecap fraction. This is comparable to the approach used to incorporate dynamic satellite data on active fires to estimate smoke fluxes for the operational NAAPS, and to the incorporation of satellite precipitation in place of numerical model outputs for reanalysis runs of NAAPS. However, AMSR2 provides limited temporal information: twice a day at 1:30 PM and 1:30 AM for its ascending and descending passes, respectively. To evaluate whether AMSR2 retrieved surface conditions persist for multiple hours, we considered the variability in surface winds from 3-hourly NAVGEM data.

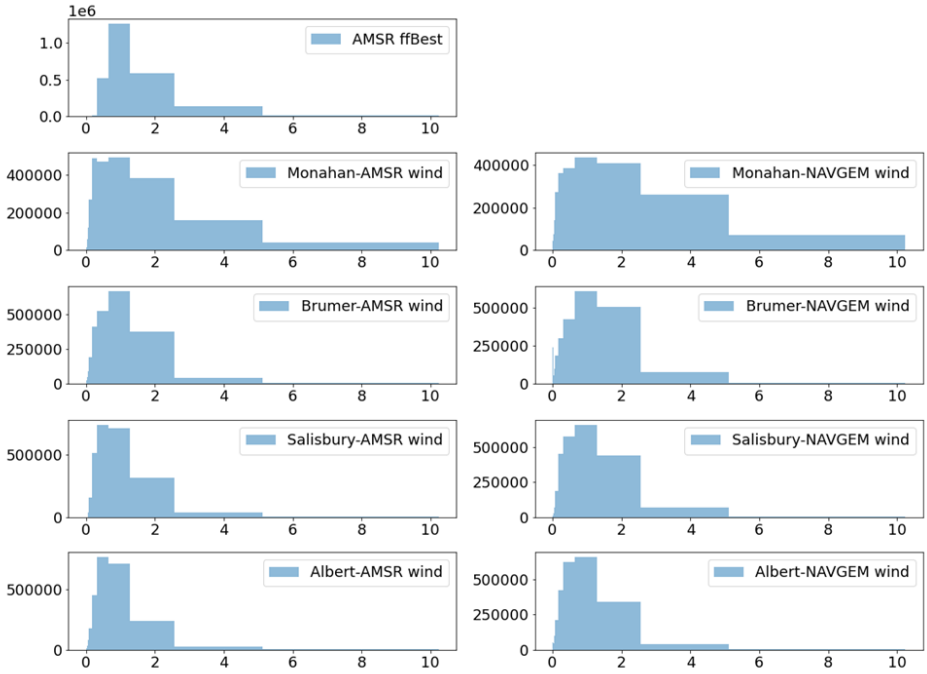

Fig. 26 — Distribution of estimated whitecap fraction *W* using the new AMSR retrieval (top), compared with parameterizations forced by AMSR retrieved winds (left) or NAVGEM forecast winds (right).

We used 8 days of NAVGEM analyses and computed the daily mean surface wind at each location, subtracting this from the instantaneous wind to obtain a sub-daily anomaly representing the approximate deviation in surface winds roughly six hours before and after a satellite overpass. Results are shown in Fig. 27. We found that some regions of high winds and high salt production in the Southern Ocean and the South China Sea have very persistent winds with low variability, while other high-wind regions, especially in the Northern Pacific, have high levels of intra-day variation, likely due to the motion of mid-latitude storm systems. The proper integration and interpolation of satellite observations to improve models by direct forcing requires careful study and quantitative testing.

6 CONCLUSIONS AND FUTURE WORK

This Memorandum report documents the work done for a NISE Type 2 project aiming to demonstrate that the use of satellite retrievals of whitecap fraction in the operational NAAPS can provide a new capability for air-sea products (Section 2) necessary for the Navy forecasts. This work is motivated by the Navy needs for improved operational models that provide predictions at multiple time scales (Section 1). Our experience with WindSat geophysical and whitecap retrievals (Section 3) justified the approach (Section 4) formulated to achieve the objectives of this project.

The achievements of the NISE project are the following:

1) Phase 1 delivered a working initial version of the whitecap algorithm using AMSR2 data (Fig. 17). The results show that the implemented code provides good proof-of-principle EDRs and *W* data from AMSR2 (Figs. 18 and 19).

2) During Phase 2, a production system was developed and tested to provide a dynamic flow of data matching AMSR2 and NWP data already used operationally by FNMOC (Fig. 21).

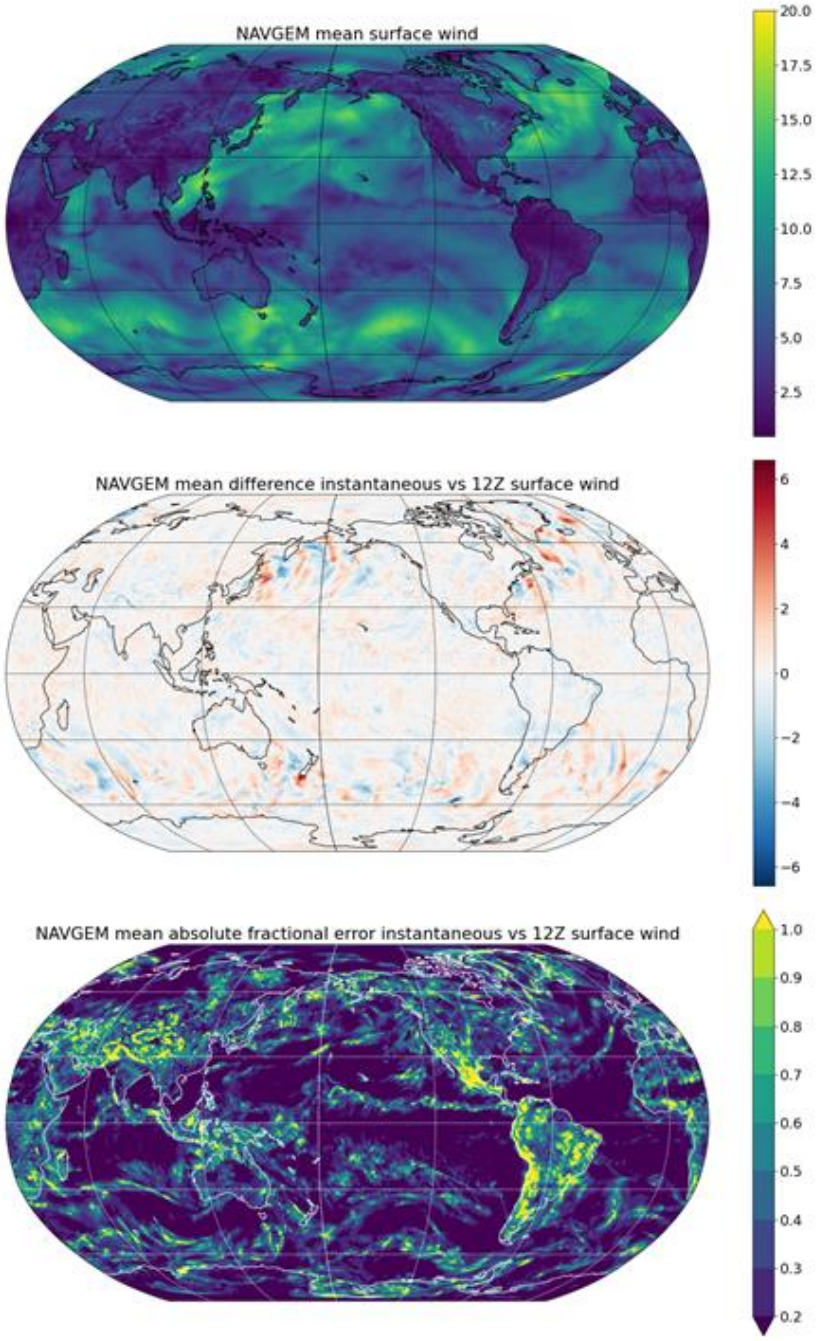

Fig. 27 — Analysis of sub-daily variation of NAVGEM surface winds. Top: Mean surface winds based on 8 days of 3-hourly NAVGEM analysis. Middle: Mean differences between the 3-hourly data and the nearest 12Z value. Bottom: Differences as an absolute fraction of the mean wind speed.

3) Using new model inputs (Section 5.2.1 and Table 3), the whitecap algorithm was improved and updated to work with both archived and near-real-time AMSR2 and NWP data (Section 5.2.2).

4) The improved whitecap algorithm with AMSR2 data provided five new products— water vapor, cloud water, 10 GHz wind speed, whitecap fraction *W*, and sea spray flux. These products were integrated into GeoIPS framework and visualized in open ocean area of the north Atlantic (Fig. 23) and at recent tropical cyclone Fiona (Fig. 24). The suite of new retrieval products is both novel and complementary to the existing satellite data products in the TCWeb (Section 5.2.5).

5) The operational NAAPS now includes three new parameterizations for the sea spray flux (Fig. 25), some of them based on satellite retrievals of the whitecap fraction (Section 3.2.2). The performance of the different parameterizations, as driven by either AMSR2 or NAVGEM wind speeds, are compared to that provided by the whitecap algorithm and AMSR2 data (Fig. 26).

6) There is additional scientific discovery supported by these new tools using this new retrieval product.

Overall, the results reported here show that this NISE project has been successful in completing the main objectives—namely, to incorporate new capability in the operational NAAPS with the potential to improve existing and add new satellite products for direct use by NAAPS as well as utilization in Navy forecast support applications.

The new capability implemented in the operational NAAPS and GeoIPS through this NISE project has potential to lead to improvements in Navy operational forecasting for a range of tactical, navigation, and aviation applications. To achieve these operational improvements, we recommend these steps:

- Systematic near-real-time generation of AMSR2 products should continue at NRL, and steps taken to reduce the latency to match conventional remote sensing retrieval products;
- Visualization of new AMSR2 products should be included in the TCWeb suite supported by NRL, and products included in informational materials and training used to inform TCWeb users;
- Archival processing of AMSR2 retrieval products should be used to examine sensitivity of whitecap fraction to environmental factors other than wind speed, with the aid of weather models;
- Using the newly implemented sea salt algorithms in NAAPS, experiments should be developed and performed to characterize 1) consistency of each algorithm with the AMSR2 retrieved values; 2) skill of each algorithm as represented by minimization of the data assimilation increment of aerosol optical depth;
- Detailed examination of the temporal variation in sea state conditions to provide forecaster guidance on use of the new AMSR2 retrieval products, and to evaluate methods for integration of AMSR2 data in NAAPS or other automated prediction systems.

With the completion of this NISE project, the Technology Readiness Level (TRL) of the whitecap retrieval algorithm has increased from 5 (component and/or breadboard validation in relevant environment) to 6 (system/subsystem model or prototype demonstration in a relevant environment). This technical maturity can support NRL-ONR-FNMOC partnership to transition air-sea interaction products for operational use via subsequent 6.2 and/or 6.4 projects (Fig. 5).

APPENDIX A: SEA SPRAY SOURCE FUNCTION

A.1 Derivation of the SSSF form used in NAAPS

Following [22], we use $W(U_{10})$ from (6), τ = 3.53 s, and dE/dr_{80} to re-write (5) as follows:

$$\frac{dF}{dr_{80}} = aU_{10}^{b}\frac{1}{\tau}\frac{dE}{dr_{80}} = U_{10}^{b}\left[\frac{a}{\tau}\frac{dE}{dr_{80}}\right] \quad \text{(A.1).}$$

Using the size distribution from [23] (their Eq. 12), we obtain the following SSSF formulation:

$$\frac{dF}{dr_{80}} = U_{10}^{3.41}\left[1.373\, r_{80}^{-3}(1+0.057 r_{80}^{1.05})\times 10^{1.19e^{-B^2}}\right] \quad \text{(A.2)}$$

where $B = (0.38 - \log r_{80})/0.65$. SSSF (A.2) is applicable for r_{80} from 0.8 to 8 μm.

Equation (A.2) is the formulation, which [22] used to obtain (4) with the following steps. First, following [24], [22] applies (A.2) for an extended r_{80} range, from 0.2 to 8 μm. Next, [22] modifies (A.2) for dry particles using the relationships $r_{80} = 2r_{dry}$ and $dF/dr_{dry} = 2\,dF/dr_{80}$. Finally, the modified, size-resolved form (A.2) is integrated over r_{dry} range of 0.2–4 μm and converted to mass flux:

$$F = \frac{4}{3}\pi\rho_{ss}\int_{0.2}^{4}\frac{dF}{dr_{\mathrm{dry}}}r_{\mathrm{dry}}^{3}dr_{\mathrm{dry}} = \frac{4}{3}\pi\rho_{ss}\int_{0.2}^{4}2\frac{dF}{dr_{80}}\left(\frac{r_{80}}{2}\right)^{3}d\left(\frac{r_{80}}{2}\right) \quad \text{(A.3)}$$

where ρ_{ss}= 2:2×10^3 [kg m^{-3}] is the dry sea salt density. The integration of (A.3) results in (4).

A.2 Size distribution in the SSSF

To see what exactly constant 3.56771×10^{-5} (in g m^{-2} s^{-1}) in (8) represents, we re-write (A.1) as follows:

$$\frac{dF}{dr_{80}} = aU_{10}^{b}\left[\frac{1}{\tau}\frac{dE}{dr_{80}}\right] \quad \text{(A.4).}$$

Denoting $W(U_{10}) = aU_{10}^{b}$ and using [23] again for τ and dE/dr_{80} (details not shown), we obtain the following expression:

$$\frac{dF}{dr_{80}} = W(U_{10})\left[3.5755\ \times10^{5}\cdot r_{80}^{-3}(1+0.057 r_{80}^{1.05})\times 10^{1.19e^{-B^2}}\right] \quad \text{(A.5).}$$

The size distribution (in the brackets) is similar to (A.2) but has a different leading constant. Integrating (A.5) as was done for (A.3), we would obtain constant 3.56771×10^{-8} in (8).

APPENDIX B: AVAILABLE AMSR2 T_B DATA

AMSR2 brightens temperature data T_B [K] are available from JAXA at three levels depending on their calibration and processing (https://www.eorc.jaxa.jp/AMSR/datacatalog/tb/). These data levels are:

- Level-1B (L1B): Product that contains T_B data over the footprint for each frequency (Table 1).
- Level-1R (L1R): Product that matches the center position and size of each footprint in each frequency band by spatial matching process.
- Level-3 (L3): Product, which is a gridded version of L1B product.

REFERENCES

1. L. Yu, 2019, "Global Air–Sea Fluxes of Heat, Fresh Water, and Momentum: Energy Budget Closure and Unanswered Questions," Annu Rev. Mar. Sci., 11, 227-248. Doi: 10.1146/annurev-marine-010816-060704
2. National Academies of Sciences, Engineering, and Medicine, 2016, "Next Generation Earth System Prediction: Strategies for Subseasonal to Seasonal Forecasts, Washington, DC, The National Academies Press. doi: 10.17226/21873.
3. M. D. Anguelova, and F. Webster, 2006, "Whitecap coverage from satellite measurements: A first step toward modeling the variability of oceanic whitecaps," Journal of Geophysical Research, 111, C03017. doi:10.1029/2005JC003158
4. G. de Leeuw, E. L Andreas, M. D. Anguelova, C. W. Fairall, E. R. Lewis, C. O'Dowd, M. Schulz, and S. E. Schwartz, 2011, "Production flux of sea spray aerosol," Rev. Geophys., 49, RG2001, doi:10.1029/2010RG000349
5. E. L Andreas, and K. A. Emanuel, 2001, "Effects of Sea Spray on Tropical Cyclone Intensity," Journal of the Atmospheric Sciences (24), 3741-3751. doi: 10.1175/1520-0469(2001)058<3741:EOSSOT>2.0.CO;2
6. Y. Wang, J. D. Kepert, and G. J. Holland, 2001, "The effect of sea spray evaporation on tropical cyclone boundary layer structure and intensity," MonWea Rev, 129: 2481–2500. doi: 10.1175/1520-0493(2001)129<2481:TEOSSE>2.0.CO;2
7. F. Veron, 2015, "Ocean spray," Annu. Rev. Fluid Mech., 47, 507–538. doi:10.1146/annurev-fluid-010814-014651
8. S. E. Brumer, C. J. Zappa, I. M. Brooks, H. Tamura, S. M. Brown, B. W. Blomquist, C. W. Fairall, and A. Cifuentes-Lorenzen, 2017, "Whitecap coverage dependence on wind and wave statistics as observed during SO GasEx and HiWinGS," J. Phys. Oceanogr., 47, 2211-2235. doi:10.1175/JPO-D-17-0005.1
9. E. C. Monahan, and I. O'Muircheartaigh, 1980, "Optimal power-law description of oceanic whitecap coverage dependence on wind speed," J. Phys. Oceanogr., 10, 2094–2099. doi:10.1175/1520-0485(1980)010<2094:OPLDOO>2.0.CO;2
10. P. W. Gaiser, K. M. St Germain, E. M. Twarog, G. A. Poe, W. Purdy, D. Richardson, et al., 2004, "The WindSat spaceborne polarimetric microwave radiometer: Sensor description and early orbit performance," Trans. Geosci. Rem. Sens., 42, 2347–2361. doi:10.1109/TGRS.2004.836867
11. M. D. Anguelova, and M. H. Bettenhausen, 2019, "Whitecap fraction from satellite measurements: Algorithm description," J. Geophys. Res, 124, 1827–1857. doi:10.1029/2018JC014630
12. M. D. Anguelova, 2016, "Assessing the utility of satellite-based whitecap fraction to estimate sea spray production and CO2 transfer velocity," IOP Conference Series: Earth and Environmental Science, 35, 012002. doi:10.1088/1755-1315/35/1/012002
13. M. Spada, O. Jorba, C. Pérez García-Pando, Z. Janjic, and J. M. Baldasano, 2013, "Modeling and evaluation of the global sea-salt aerosol distribution: sensitivity to size-resolved and sea-surface temperature dependent emission schemes," Atmos. Chem. Phys., 13, 11735–11755. doi:10.5194/acp-13-11735-2013
14. Potter, H., G. B. Smith, C. M. Snow, D. J. Dowgiallo, J. P. Bobak, and M. D. Anguelova**,** 2015, "Whitecap lifetime stages from infrared imagery with implications for microwave radiometric measurements of whitecap fraction," J. Geophys. Res., 120, 7521-7537. doi:10.1002/2015JC011276

15. M. H. Bettenhausen, and M. D. Anguelova**,** 2019, "Brightness Temperature Sensitivity to Whitecap Fraction at Millimeter Wavelengths," Remote Sensing, 11(17), 2036. doi:10.3390/rs11172036

16. M. H. Bettenhausen, C. K. Smith, R. M. Bevilacqua, N.-Y. Wang, P. W. Gaiser, and S. Cox, 2006, "A nonlinear optimization algorithm for WindSat wind vector retrievals," Trans. Geosci. Remote Sens., 44(3), 597-610. doi:10.1109/TGRS.2005.862504

17. M. D. Anguelova, and P. W. Gaiser, 2012, "Dielectric and radiative properties of sea foam at microwave frequencies: Conceptual understanding of foam emissivity," Remote Sensing, 4, 1162-1189. doi:10.3390/rs4051162

18. K. St. Germain, G. Poe, and P. Gaiser, 2002, "Polarimetric emission model of the sea at microwave frequencies and comparison with measurements," Prog. Electromagn. Res., 37, 1– 30. doi:10.2528/PIER01100800

19. J. T. Johnson, J. T., 2006, "An efficient two-scale model for the computation of thermal emission and atmospheric reflection from the sea surface," Trans. Geosci. Remote Sens., 44(3), 560–568. doi:10.1109/TGRS.2005.855999

20. X. Liu, and J. Duncan, 2003, "The effects of surfactants on spilling breaking waves," Nature 421**,** 520–523. doi:10.1038/nature01357

21. M. D. Anguelova, and P. W. Gaiser, 2013, "Microwave emissivity of sea foam layers with vertically inhomogeneous dielectric properties," Remote Sensing of Environment, 139, 81–96. doi:10.1016/j.rse.2013.07.017

22. Witek, M. L., P. J. Flatau, P. K. Quinn, and D. L. Westphal, 2007, "Global sea-salt modeling: Results and validation against multicampaign shipboard measurements," J. Geophys. Res., 112, D08215. doi:10.1029/2006JD007779

23. E. C. Monahan, D. E. Spiel, and K. L. Davidson, 1986, "A model of marine aerosol generation via whitecaps and wave disruption," in *Oceanic whitecaps and their role in air-sea exchange processes*, E. C. Monahan, and G. Mac Niocaill (D. Reidel Publishing Company, Dordrecht, the Netherlands) 167–174.

24. E. C. Monahan, and I. O'Muircheartaigh, 1980, "Optimal power-law description of oceanic whitecap coverage dependence on wind speed," J. Phys. Oceanogr., 10, 2094–2099.

25. S. L. Gong, 2003, "A parameterization of sea-salt aerosol source function for sub- and super-micron particles," Global Biogeochem. Cy., 17, 1097. doi:10.1029/2003GB00207903

26. D. J. Salisbury, M. D. Anguelova, and I. M. Brooks, 2013, "On the variability of whitecap fraction using satellite-based observations," J. Geophys. Res.-Oceans, 118, 6201–6222.

27. J I. Rubin, J S. Reid, J A. Hansen, J L. Anderson, N. Collins, T. J. Hoar, T. Hogan, P. Lynch, J. McLay, C. A. Reynolds, W. R. Sessions, D. L. Westphal, J. L. Zhang, 2016, "Development of the Ensemble Navy Aerosol Analysis Prediction System (ENAAPS) and its application of the Data Assimilation Research Testbed (DART) in support of aerosol forecasting," Atm. Chem. Phys., 16, 3927-3951.

28. J. I. Rubin, J. S. Reid, J. A. Hansen, J. L. Anderson, B. N. Holben, P. Xian, D. L. Westphal, J. L. Zhang, 2017, "Assimilation of AERONET and MODIS AOT observations using variational and ensemble data assimilation methods and its impact on aerosol forecasting skill," J. Geophys. Res, 122, 4967-4992.

29. M. F. M. A. Albert, M. D. Anguelova, A. M. M. Manders, M. Schaap, and G. de Leeuw, 2016, "Parameterization of oceanic whitecap fraction based on satellite observations," Atm. Chem. Phys, 16(21), 13,725–13,751. doi: 10.5194/acp-16-13725-2016

30. S. Remy, and M. D. Anguelova, 2021, Improving the Representation of Whitecap Fraction and Sea Salt Aerosol Emissions in the ECMWF IFS-AER, Remote Sensing, 13, 4856. doi:10.3390/rs13234856

31. T.F. Hogan, M. Liu, J.A. Ridout, M.S. Peng, T.R. Whitcomb, B.C. Ruston, C.A. Reynolds, S.D. Eckermann, J.R. Moskaitis, N.L. Baker, J.P. McCormack, K.C. Viner, J.G. McLay, M.K. Flatau, L. Xu, C. Chen, and S.W. Chang, 2014, "The Navy Global Environmental Model," Oceanography 27(3):116–125. doi:10.5670/oceanog.2014.73

32. Weather and climate models at National Centers for Environmental Information, NOAA: https://www.ncei.noaa.gov/products/weather-climate-models/frnmoc-navy-global-hybrid-ocean

33. J. Zhang, J. S. Reid, D. L. Westphal, N. L. Baker, and E. J. Hyer, 2008, "A system for operational aerosol optical depth data assimilation over global oceans," J. Geophys. Res., 113, D10208. doi:10.1029/2007JD009065

34. J-M. Lellouche, O. Legalloudec, C. Regnier, B. Levier, E. Greiner, and M. Drevillon, 2019, "Quality information document for global sea physical analysis and forecasting product global analysis forecast phy 001 024 (Tech. Rep. Issue: 2.1): EU Copernicus Marine Service. https://oceanrep.geomar.de/46419/1/CMEMS-GLO-QUID-001-024.pdf

35. T. Meissner and F. J. Wentz, 2012, "The emissivity of the ocean surface between 6 and 90 GHz over a large range of wind speeds and earth incidence angles," Trans. Geosci. Remote Sens., 50(8), 3004-3026. doi:10.1109/TGRS.2011.2179662